Environmental Science & Technology

Article

pubs.acs.org/est

Incorporation and Retention of 99-Tc(IV) in Magnetite under High pH Conditions

Timothy A. Marshall,[†] Katherine Morris,*[,†] Gareth T. W. Law,[‡] J. Frederick W. Mosselmans,[§] Pieter Bots,[†] Stephen A. Parry,[§] and Samuel Shaw[†]

[†]Research Centre for Radwaste Disposal and Williamson Research Centre for Molecular Environmental Science, School of Earth, Atmospheric and Environmental Sciences, The University of Manchester, Manchester, M13 9PL, United Kingdom

[‡]Centre for Radiochemistry Research and Research Centre for Radwaste and Decommissioning, School of Chemistry, The University of Manchester, Manchester, M13 9PL, United Kingdom

[§]Diamond Light Source Ltd., Harwell Science and Innovation Campus, Didcot, Oxfordshire OX11 0DE, United Kingdom

Supporting Information

ABSTRACT: Technetium incorporation into magnetite and its behavior during subsequent oxidation has been investigated at high pH to determine the technetium retention mechanism(s) on formation and oxidative perturbation of magnetite in systems relevant to radioactive waste disposal. Ferrihydrite was exposed to $Tc(VII)_{(aq)}$ containing cement leachates (pH 10.5−13.1), and crystallization of magnetite was induced via addition of $Fe(II)_{aq}$. A combination of X-ray diffraction (XRD), chemical extraction, and X-ray absorption spectroscopy (XAS) techniques provided direct evidence that Tc(VII) was reduced and incorporated into the magnetite structure. Subsequent air oxidation of the magnetite particles for up to 152 days resulted in only limited remobilization of the incorporated Tc(IV). Analysis of both X-ray absorption near edge structure (XANES) and extended X-ray absorption fine structure (EXAFS) data indicated that the Tc(IV) was predominantly incorporated into the magnetite octahedral site in all systems studied. On reoxidation in air, the incorporated Tc(IV) was recalcitrant to oxidative dissolution with less than 40% remobilization to solution despite significant oxidation of the magnetite to maghemite/goethite: All solid associated Tc remained as Tc(IV). The results of this study provide the first direct evidence for significant Tc(IV) incorporation into the magnetite structure and confirm that magnetite incorporated Tc(IV) is recalcitrant to oxidative dissolution. Immobilization of Tc(VII) by reduction and incorporation into magnetite at high pH and with significant stability upon reoxidation has clear and important implications for limiting technetium migration under conditions where magnetite is formed including in geological disposal of radioactive wastes.

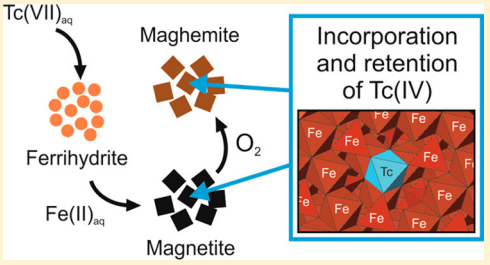

INTRODUCTION

Technetium-99 (Tc-99) is a long-lived radioactive fission product (half-life 2.1×10^5 years) present in many spent fuel and reprocessing derived radioactive wastes. The environmental mobility of Tc-99 in the subsurface is primarily governed by its oxidation state. Under oxidizing conditions, Tc(VII) is highly soluble (~11 M)[1] and environmentally mobile, existing as the pertechnetate, TcO_4^-, anion. In contrast, under reducing conditions, Tc(IV) is dominant and generally precipitates as sparingly soluble Tc(IV)-hydroxide phases (10^{-8}−10^{-9} M)[2−4] or adsorbs to mineral surfaces.[5−8] Due to its high mobility under oxic conditions and its long half-life, Tc-99 is a significant risk driving radionuclide for geological disposal of radioactive wastes, as well as presenting a significant challenge to remediation of radioactively contaminated land[9] in the UK,[10,11] the USA,[12−14] and Russia.[15] Past work has shown that Fe(II) bearing oxides[16−18] and sulfides[19−21] are effective in removing Tc(VII) from solution via reductive adsorption or precipitation. In addition, Fe(II) adsorbed to mineral surfaces such as iron or aluminum (oxyhydr)oxides has also been shown to be a highly effective abiotic reductant for Tc(VII).[17,22,23] Microbially mediated reduction of Tc(VII) has also been documented, with enzymatic and indirect (via reaction with biogenic Fe(II)) pathways possible but with indirect reduction dominating.[6,24−26] Although aqueous Fe(II) is able to reduce Tc(VII), the kinetics of this pathway are relatively slow.[27] In general, the reductive ability of Fe(II) increases from aqueous Fe(II) to structural Fe(II) to adsorbed Fe(II).[9] Reflecting this, transport of Tc-99 in the environment will therefore be significantly controlled by the Tc-99 interactions with Fe(II) bearing solid minerals (e.g., iron oxides, sulfides) through either sorption[8,28] or surface mediated reduction and precipitation.[29,30]

Exposure of reduced Tc-99-bearing sediments to oxidizing conditions may induce remobilization of Tc(VII) back into

Received: July 16, 2014
Revised: September 17, 2014
Accepted: September 19, 2014
Published: September 19, 2014

solution, although the extent of remobilization will be dependent upon both the binding mechanism and the oxidant. Sediments labeled with Tc-99 from authorized effluent discharges from Sellafield showed evidence that Tc-99 is retained on sediments over periods of decades even in dynamic saltmarsh environments.[31] Laboratory based studies on remobilization of Tc-99 in shallow sediments indicated that, after Fe(III)-reducing conditions had developed and Tc(VII) was reductively scavenged to sediments, upon oxidation a variable fraction of the sediment associated Tc-99 was recalcitrant to oxidative remobilization.[32−35] Under certain conditions, oxidative exposure to air caused remobilization of >50% of the sediment associated Tc(IV) over several months.[12,33,36] Further, a study on iron minerals by Wharton et al.[19] reported Tc-99 remaining as Tc(IV) despite oxidation of associated mackinawite (tetragonal FeS) to goethite in air. In these studies, the potential existed for Tc(IV) to be incorporated within the oxidized secondary mineral phases, potentially contributing to its recalcitrance to oxidative remobilization.

Incorporation of technetium into stable mineral phases, such as iron (oxyhydr)oxides, offers a pathway for Tc sequestration with the potential for immobilization. Indeed, evidence for Tc(IV) incorporation into goethite (α-FeOOH) during coprecipitation has been reported,[37,38] and Tc(IV) incorporation to hematite (α-Fe_2O_3) has been predicted from modeling.[39] Both these studies suggest that Tc(IV) can be octahedrally coordinated within the relevant crystal structure and can directly substitute for Fe(III). Products of steel corrosion (magnetite, maghemite, and goethite) have also been shown to be able to partially reduce Tc(VII) to Tc(IV), with the authors concluding the Tc-99 was incorporated into the corroded steel surface.[40] It has also been recently suggested that adsorbed Tc(IV) may, with time, become incorporated into the magnetite (Fe_3O_4) structure.[41] It is clear that the reductive incorporation of Tc-99 as Tc(IV) into magnetite under environmental conditions relevant to contaminated sites and geodisposal of wastes could significantly reduce the mobility of Tc-99. However, the mechanism of Tc-99 incorporation into the structure of magnetite and the amount and mechanism of release during oxidation remains unknown.

Crystallization of ferrihydrite to magnetite proceeds via sorption of Fe(II) onto ferrihydrite followed by a solid-state transformation between ferrihydrite, goethite, and magnetite and with additional growth of already nucleated magnetite particles.[42−44] At low solution Fe(II) concentrations (<0.03 mmol/L), only goethite precipitates, with nucleation of magnetite increasing with increasing Fe(II) concentration and with magnetite crystallization eventually proceeding at the expense of goethite.[42−44] Magnetite oxidizes to maghemite (γ-Fe_2O_3) topotactically through outward diffusion of Fe, with no change in the crystal size or shape and the creation of 2.67 cation vacancies per unit cell.[45] This process initially leads to the formation of a pure Fe(III) surface layer on the magnetite particle which increases in thickness until the entire particle has transformed to maghemite.[45] The identity of the Fe species undergoing outward diffusion during this process is not agreed upon in the literature, although Fe(II) is the more favored.[45−47] Understanding the potential for incorporation of technetium into magnetite during its formation and oxidation and under conditions relevant to radioactive waste disposal is the focus of this study.

Many geodisposal concepts utilize cementitious materials in the design of a deep geological disposal facility (GDF), for example, as part of the engineered barrier system or as structural materials. Leaching of these materials upon resaturation will buffer the pH to hyperalkaline conditions (pH 10.5−13.1), creating a plume of alkaline fluid in the host rock and/or local environment.[48] Furthermore, hyperalkaline conditions can prevail in many contaminated land scenarios, e.g., where cementitious building materials contact subsurface sediments[49,50] and at the underground waste storage tanks at the Hanford Site in Washington State, USA, where there has been considerable attention focused on behavior of Tc-99.[13,14,39,51−53] Additionally, microbial reduction of Fe(III) leading to the formation of magnetite has recently been shown to occur under alkaline conditions,[54] highlighting the importance of biogeochemistry in these processes and lending further significance to the work in this contribution.

The aim of this study was to characterize the mechanism(s) of Tc-99 reaction with magnetite as it crystallizes under alkaline conditions, to determine whether significant amounts of Tc-99 could be incorporated into this environmentally important phase and to explore the effects of oxidative perturbations on Tc-99 speciation and solubility. The system we have explored is crystallization of ferrihydrite as an initial Fe(III) oxyhydroxide product to magnetite by addition of aqueous Fe^{2+}.[42] We followed the partitioning of Tc(VII) during this process in three synthetic cement leachates (pH 10.5, 12.5, and 13.1). After a period of aging, the Tc-99 doped magnetite systems were then exposed to oxidizing conditions to test the recalcitrance of any iron oxide associated Tc-99 to reoxidation and thus to explore the stability of the radionuclide. We have combined geochemical data with quantitative powder X-ray diffraction (QXRD), transmission electron microscopy (TEM) and energy dispersive X-ray spectroscopy (EDX), and X-ray absorption spectroscopy (XAS) to thoroughly characterize the fate of Tc-99 during magnetite crystallization and reoxidation at high pH. Throughout, we have focused on the fate of Tc-99: first, during ferrihydrite crystallization to magnetite, we determined the extent of Tc-99 incorporation and defined its atomic scale bonding environment; we then oxidized the Tc-99-labeled magnetite over several months to determine if incorporation offered protection against oxidative remobilization.

MATERIALS AND METHODS

Batch experiments were used to follow the Fe(II)-mediated crystallization of ferrihydrite to magnetite[42−44] in three Tc(VII) amended synthetic cement leachates (CL), chosen to simulate a young (YCL, pH 13.1), intermediate (ICL, pH 12.5), and old (OCL, pH 10.5) postclosure groundwater around a GDF.[48,55] Details on preparation of the cement leachates are given in the Supporting Information. Parallel experiments were also set up without Tc(VII) present to allow characterization of the solid products by X-ray diffraction (XRD). The 2-line ferrihydrite used as a starting material was synthesized as per Cornell and Schwertmann,[56] and the Fe(III) content of the resultant paste was determined by dissolution in 1 M HCl and analysis by the ferrozine method.[57] A known quantity of ferrihydrite was equilibrated with the cement leachates at a solid/solution ratio of 3.5 g L^{-1} for 1 h on an orbital shaker at room temperature in an anaerobic chamber (5% H_2, balance N_2, maintained at <1 ppm of O_2 and CO_2). After equilibration with the ferrihydrite, the pH was manually readjusted to the initial leachate pH by

Table 1. Quantitative Analysis of XRD Patterns from Reduced and Air Oxidized Solid Products in Synthetic Young (YCL, pH 13.1), Intermediate (ICL, pH 12.5), and Old (OCL, pH 10.5) Cement Leachates

experiment		magnetite unit cell length (Å)	magnetite stoichiometry[a] (Fe^{2+}/Fe^{3+})	magnetite crystallite size (Å)	weight % magnetite	weight % goethite
YCL	reduced	8.400 (0)	0.53 (5)	35 (2)	74.2 (6)	25.8 (6)
(pH 13.1)	21 day oxidized	8.394 (0)	0.47 (4)	33 (2)	73.5 (6)	26.5 (6)
	152 day oxidized	8.386 (1)	0.39 (5)	34 (5)	52 (2)	47 (2)
ICL	reduced	8.391 (1)	0.45 (5)	19.2 (6)	79.9 (9)	20.3 (9)
(pH 12.5)	21 day oxidized	8.378 (1)	0.33 (4)	19.2 (6)	75.2 (7)	24.8 (7)
	152 day oxidized	8.356 (1)	0.12 (3)	15 (1)	51 (1)	49 (1)
OCL	reduced	8.393 (1)	0.46 (5)	22.5 (7)	100	
(pH 10.5)	21 day oxidized	8.377 (1)	0.32 (4)	21.8 (7)	100	
	152 day oxidized	8.365 (1)	0.21 (4)	21 (2)	52 (2)	48 (2)

[a]Magnetite stoichiometry was calculated from unit cell length using the method of Gorski and Scherer.[63] Numbers in parentheses are 1 standard deviation error on the last significant figure. Blank cells indicate that the structure was omitted from the refinement.

addition of KOH. Tc(VII) was then added to the experiments as ammonium pertechnetate (NH_4TcO_4) to give an initial solution concentration of 3 ppm (30.3 μM, 2 kBq ml^{-1}). Crystallization to magnetite was then induced by addition of Fe(II) as 0.1 M $FeCl_2$, to give stoichiometric magnetite with an Fe(II)/Fe(III) ratio of 1:2. After Fe(II)-addition, the pH was immediately readjusted to the initial leachate pH using KOH. The alkaline magnetite suspension was then aged for 2 days in the anaerobic chamber. Following this, the experiments were moved to a separate glovebag containing CO_2-free air (Zero grade Air) where they were allowed to oxidize for up to 152 days. A further experiment was set up in the intermediate stage cement leachate (ICL, pH 12.5) as a sorption "control" where the Tc-99 was spiked to preformed magnetite after 1 day. After a further day of reaction, a subsample of the experiment was then transferred to the glovebag containing CO_2-free air for 152 days for oxidation. All experiments were shaken on an orbital shaker (150 rpm) to allow exchange with the relevant atmosphere (i.e., reducing: H_2/N_2 mix; oxidizing: CO_2-free air) but were not purged with the relevant gas. Minor aggregation of particles was observed in all three systems over time. The pH was periodically monitored throughout the experiments, and no further pH adjustment was required after the initial pH was set.

Partitioning of Tc-99 between the solid/solution was determined by analysis of a 1 mL solution aliquot for Tc-99 by liquid scintillation counting (LSC) using a Packard Tricarb 2100TR liquid scintillation analyzer. The distribution of Tc-99 within the magnetite particles and oxidized products was determined by total digestion in 1 M HCl where the relative dissolution rate of Tc-99 versus total Fe in the acidic leachate provided insight into the concentration gradient of Tc-99 through the solid. The mineral sample was allowed to fully dissolve in the acid, with the resultant solution analyzed at selected time points during dissolution. Samples were analyzed for Tc-99 using LSC and Fe by the ferrozine method[57] until no further increase in the concentration of Fe in the acidic solution was observed. Full details of the method are included in the Supporting Information. Where appropriate, selected samples were characterized by XRD using a Bruker D8 diffractometer (λ = Cu K-α1). For TEM, solid samples were characterized using an FEI CM200 Field Emission Gun TEM, operating at 197 kV and fitted with a Gatan Imaging Filter (GIF 200) and an Oxford Instruments Silicon Drift Detector EDX spectrometer running AZTEC software. Tc-99 K-edge XAS spectra were collected on Beamline B18, at the Diamond Light Source[58] at room temperature in fluorescence mode using a 9-element Ge detector.[59] Data reduction and fitting of the X-ray absorption fine structure (EXAFS) spectra were performed using the software packages Athena and Artemis.[60]

RESULTS AND DISCUSSION

Characterization of the Iron Oxide Products. XRD patterns show that, after 2 days of aging, magnetite was the dominant product formed in each of the leachates (Figure SI-1, Supporting Information) but that in the YCL (pH 13.1) and ICL (pH 12.5) experiments goethite was also formed (QXRD analysis suggested up to 20−25%, Table 1). In contrast, the pH 10.5 OCL product was magnetite only (Figure SI-1, Supporting Information, Table 1). During the oxidation experiments, the color of solids changed from black to brown in all leachates suggesting that oxidation of the magnetite had occurred. After 21 days of oxidation in CO_2-free air, the XRD patterns for all experiments were the same as the fully reduced samples within error and with no significant increase in the goethite present in the YCL and ICL systems and no measurable ingrowth of goethite into the OCL system (Figure SI-1, Supporting Information, Table 1). However, after 152 days of oxidation, all three samples contained approximately 50% goethite as expected for magnetite oxidation at high pH (Figure SI-1, Supporting Information, Table 1).[61] Oxidative maghematisation was evident from a shift in the magnetite (511) and (440) peaks in the XRD pattern to higher 2θ in the 152 days of oxidation in both the ICL and OCL experiments, in agreement with the QXRD data (Figure SI-2, Supporting Information). However, the characteristic maghemite (210) and (211) peaks[62] were not observed (Figure SI-2, Supporting Information), indicating only partial maghematisation has occurred. The length of the unit cell *a* axis dimension has previously been used as a measure of stoichiometry, i.e., Fe(II)/Fe(III) ratio.[63] Stoichiometric magnetite has an Fe(II)/Fe(III) ratio of 0.5 which decreases to zero in maghemite, while the unit cell length decreases from 8.396 to 8.340 Å.[56,64] In the 152 day samples, a shortening of the unit cell length was observed in all three systems indicating a decrease in the Fe(II)/Fe(III) ratio consistent with oxidation (Table 1). Using the stoichiometric method of Gorski and Scherer,[63] we have calculated the Fe(II)/Fe(III) ratio and, hence, the degree of maghematization, for our samples (Table 1). After 152 days of oxidation, complete oxidation of the three experiments had not occurred; the lowest Fe(II)/Fe(III) ratio and hence greatest extent of maghematization was observed in the ICL system (0.12 ± 0.03), while the

least extent of maghematization was in the YCL system (0.39 ± 0.05). Complete oxidation of maghemite nanoparticles in aqueous systems has been observed to occur over approximately three months[46] suggesting that, in our alkaline systems, magnetite has a degree of recalcitrance to oxidation. Incorporation of trace elements into magnetite (e.g., Co, Ni, Zn, up to 1 wt %) has previously been suggested to stabilize Fe(II) and suppress maghematisation through a decrease in electron mobility.[45] The incomplete maghematization observed in our samples despite almost double the oxidation time compared to the past study[46] could potentially indicate incorporation of Tc(IV) and stabilization of Fe(II) within the magnetite structure in the immediate vicinity of Tc(IV) as a charge compensation mechanism and which may inhibit complete oxidation.

TEM images (Figures SI-3 and SI-4, Supporting Information) confirmed the presence of crystalline nanoparticulate magnetite (angular to rounded cubes and rhombs, 5−20 nm in size) and goethite (needles) in the reaction products. Tc-99 was not detected using energy dispersive X-ray spectroscopy (EDX) in any of the samples analyzed, suggesting the Tc-99 was distributed throughout the sample rather than as a discrete phase and/or the Tc-99 concentration was below the limit of detection for this technique.

Technetium removal from solution to the solid during magnetite formation and oxidation is shown in Figure 1.

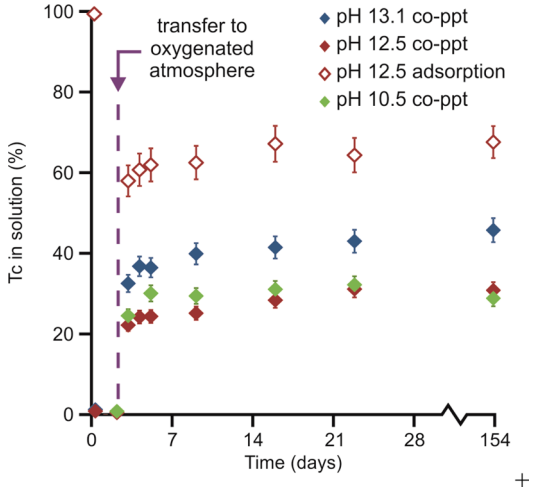

Figure 1. Removal of Tc-99 from solution (%) during magnetite aging (days 0−2) and subsequent oxidative remobilization of Tc-99 to solution during air oxidation (days 3−154) in young (YCL, pH 13.1), intermediate (ICL, pH 12.5), and old (OCL, pH 10.5) cement leachates. Closed blue diamonds = YCL coprecipitation; closed red diamonds = ICL coprecipitation; open red diamonds = ICL sorption; closed green diamonds = OCL coprecipitation.

Regardless of pH, all Tc-99 was removed from solution to below detection limit (ca. 0.5 Bq ml^{-1}; 0.8 ppb) within minutes after the addition of Fe(II) and with no release back to solution during aging. Upon oxidation in air, there was an initial rapid remobilization of Tc-99 to solution over the first day with a continued slow release over the first 2 weeks; however, the Tc-99 concentration in solution then remained essentially constant. The total amount of oxidative release of Tc-99 was dependent upon the solution composition. The Tc-99 released in the OCL (pH 10.5) and ICL (pH 12.5) systems was similar with ∼20% of Tc-99 released after 1 day of oxidation rising to ∼30% after 152 days. In the YCL, the release profile was similar, but the total release was higher, at ∼30% after 1 day rising to ∼40% after 152 days. The greater extent of Tc-99 released to solution in the YCL compared to the ICL and OCL may be due to increased oxidation of the magnetite surface at higher pH.[61] In addition, differential aggregation of the particles could potentially influence the Tc(IV) remobilization behavior. However, the particle aggregation on reoxidation was similar for each leachate and seems not to explain the differential remobilization across the different cement leachates and the persistently greater remobilization in the YCL. In contrast, in the adsorption experiment where Tc-99 was adsorbed to preformed magnetite at pH 12.5 in ICL, greater oxidative remobilization was observed compared to the coprecipitated experiments with ∼70% of the Tc-99 oxidatively remobilized to solution after 152 days. In the reoxidation experiment with the adsorbed sample, the remaining ∼30% of Tc-99 was in some way recalcitrant to air oxidation and was retained by the solid phase even though Tc(VII) was exposed to the preformed Fe(II)-bearing mineral. Interestingly, similar behavior has been observed for reduction of Tc-99 onto preformed magnetite, where EXAFS analysis suggested some incorporation of Tc-99 into the magnetite after aging.[41]

Technetium Distribution within the Solids. Magnetite dissolves isotropically allowing the distribution profile of trace elements within the solid to be assessed by acid digestion.[65,66] We performed 1 M HCl digestions on the samples from the OCL (pH 10.5) experiment to explore the Tc-99 distribution profile in the solid since these contained negligible goethite implying that all Tc-99 measured would be from magnetite associated Tc-99 (Figure 2). The dissolution profile of Tc-99 vs

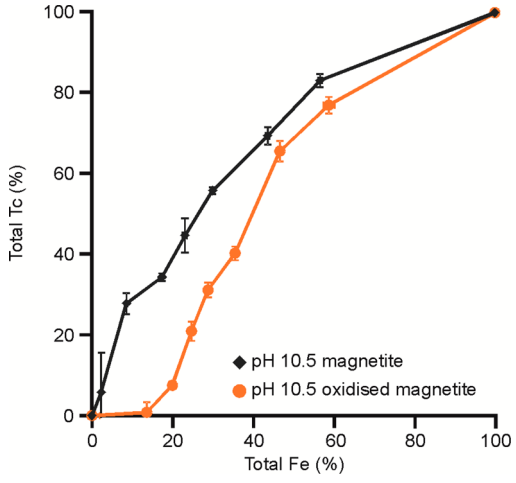

Figure 2. Tc-99 release to solution from solids versus total Fe release to solution in a 1 M HCl leach of magnetite coprecipitated with Tc-99 in old cement leachate (pH 10.5). Black diamonds = reduced magnetite; orange circles = 21 day air oxidized magnetite.

Fe in the reduced sample had a gradient initially greater than 1 which then fell to less than 1 when more than 50% of the available Fe was dissolved. This indicated that Tc-99 was not uniformly distributed through the magnetite particles and was relatively concentrated at the surface, an effect previously observed for Mn(II) and Cu(II).[65,66] The OCL oxidized mineral sample from 21 days, which showed no ingrowth of secondary goethite, showed that approximately 10% of the Fe in the sample was dissolved before any Tc-99 was detected in

solution, suggesting the development of an Fe rich/Tc-99 poor rind during oxidation. After this, the Tc-99 and Fe profiles were similar to the magnetite sample with an initial slope greater than 1, and after approximately 50% Fe dissolution, the gradient fell to below 1 reflecting an apparently heterogeneous distribution of Tc-99. From the Tc-99 distribution profile of the reduced OCL magnetite sample, 30% Tc-99 was dissolved in the acid by the time only 10% Fe had dissolved (Figure 2) suggesting that 30% of the Tc-99 released to solution during oxidation (Figure 2) can be explained by release of Tc-99 from the outer 10% of the 1 M HCl leachable magnetite particles.

X-ray Absorption Spectroscopy. X-ray absorption near edge structure (XANES) and EXAFS spectra were collected from the reduced magnetite and two oxidized samples (21 and 152 days) from coprecipitation experiments in each cement leachate, along with the sorption sample in ICL (pH 12.5). It was not possible to collect XAS data for the 21 day oxidized sorption sample as it was found that the Tc-99 concentration was too low for analysis. The edge position of all the XANES spectra aligned to the Tc(IV) reference,[67] and there was no evidence in any samples for the distinctive Tc(VII) pre-edge peak at 21045−21050 eV (Figure 3). A linear combination fit

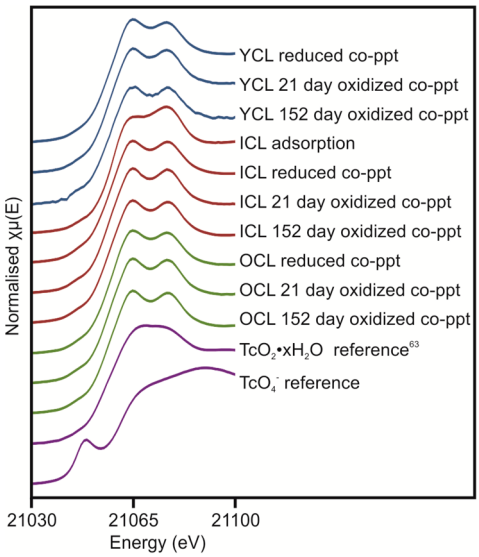

Figure 3. Technetium K-edge XANES spectra from Tc-99 incorporated into reduced and oxidized magnetite in young (YCL, pH 13.1), intermediate (ICL, pH 12.5), and old (OCL, pH 10.5) cement leachates.

between the oxic and reduced reference spectra resulted in no (0%) contribution from Tc(VII) to each of the experimental spectra (Table SI-1, Supporting Information). This indicated that Tc(VII) was fully reduced to Tc(IV) in each system and that, for reoxidized samples, any Tc-99 that remained associated with the solid was retained as Tc(IV) throughout air oxidation. The distinct double peak observed in the near edge of each of the sample spectra, which is absent from the TcO_2 reference, has previously been attributed to the presence of Tc−Fe bonds.[40]

The EXAFS spectra collected from samples in the ICL system (pH 12.5) are plotted in Figure 4, along with the nonlinear least-squares fits to the data. It is clear that the Tc-99 in the sorption sample (Figure 4) is in a very different coordination environment when compared to the coprecipitation samples, with a single wave dominating the *k*-space in the sorption system. The relatively weak second peak in the Fourier transform at approximately 3.5 Å suggests there are few absorbers/scatterers in the second shell suggesting the Tc-99 was predominantly present on the magnetite surface. Interestingly, all of the ICL coprecipitation samples are strikingly similar including the 21 and 152 day oxidized samples (Figure 4). This confirms that air oxidation had very little effect on the Tc-99 local bonding environment in these samples, even after 152 days. In the coprecipitation systems, again there was similarity across the reduced and oxidized samples and it is also clear that in all the samples the second shell of scattering atoms contributed more strongly to the EXAFS compared to the parallel sorption sample. This was confirmed by intense peaks in the phase-shifted Fourier transform of all three coprecipitation samples in the 2.5−4 Å range indicating a large number of backscattering atoms in these shells and suggesting incorporation of Tc(IV) into the magnetite structure.

Previously, Tc(IV) reduced onto environmental surfaces has been fitted using polymeric Tc chains[22,51,52] or hydrous TcO_2 like phases,[26] and both of these models can be applied to our magnetite sorption data with similar results. In the reduced and oxidized sorption samples, the addition of either Tc-99 or Fe shells beyond the Tc−O shell did not significantly improve the fit, and F-tests[68] confirmed the more complex fits were statistically indistinct from a single Tc−O shell fit (Figure SI-5 and Tables SI-2 to SI-4, Supporting Information). Therefore, the best fit to the sorption sample was an averaged TcO_2 structure, as expected for an amorphous hydrous-TcO_2 precipitate on the magnetite surface. Interestingly, the double peak in the XANES region in all samples suggests the presence of Tc−Fe bonds.[40] The presence of this feature in the magnetite sorption samples may indicate a component of a Tc−Tc chain sorbed to the magnetite surface[22] or indeed some incorporation of Tc(IV) into the magnetite, as postulated previously[41] and supported by the Tc-99 solution data (Figure 1).

The Tc-99 EXAFS from the coprecipitation samples were fitted assuming a model of Tc(IV) incorporation into the magnetite structure where Tc(IV) was substituted solely into the octahedral site and similar to the model for Ti(IV) substitution into magnetite.[18] In our model, the Tc−O coordination was fixed at 6 while the coordination of the two Tc−Fe shells was allowed to vary. This approach achieved a good fit with interatomic distances similar to those for octahedrally coordinated Fe(III) in pure magnetite[69] (Table 2). The Tc−Fe coordination in both shells was lower than, although within error of, the expected coordination of 6, with 4.7 ± 1.3 and 4.4 ± 1.3 in the Tc−Fe shells. In nanoparticulate systems, surface effects may result in lower coordination numbers; atoms residing in the near-surface of a particle will have a lower coordination in the metal−metal shells than those in the particle core. This effect has previously been observed for U−U coordination in uraninite nanoparticles.[70] We have shown that, in our reduced samples, Tc-99 was relatively concentrated in the near-surface of iron oxide nanoparticles, which suggests surface effects may explain the observed low Tc−Fe coordination. The EXAFS data and associated fits from the reduced and oxidized magnetite in the YCL (pH 13.1) and OCL (pH 10.5) systems are within error of those in the ICL (pH 12.5) system (Figure SI-6 and Table SI-5, Supporting Information).

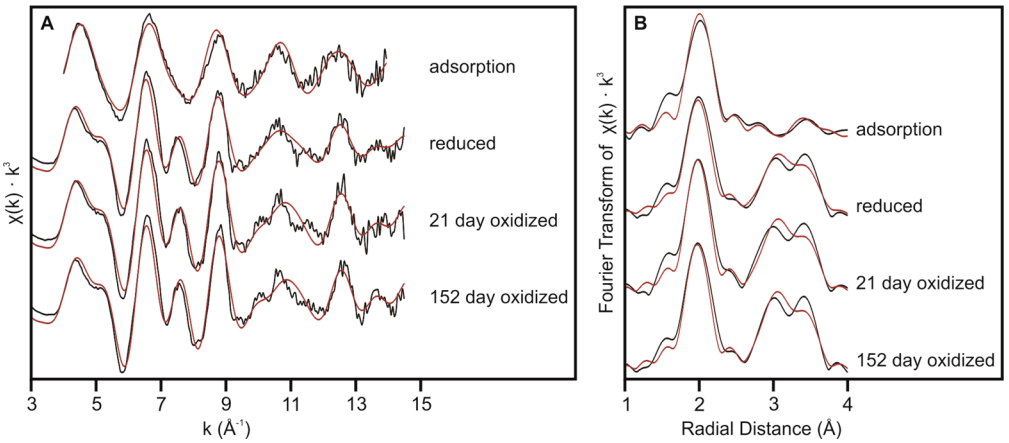

Figure 4. Technetium K-edge XAS spectra from Tc-99 adsorbed to and coprecipitated with magnetite and subsequent air oxidation in the Intermediate Cement Leachate (ICL, pH 12.5). Panel A, k^3-weighted EXAFS; panel B, Fourier transform of k^3-weighted EXAFS, using a Hanning window function and plotted with phase shift calculated from the Tc−O path. Black lines are data, and red lines represent best fit models for the data.

Table 2. Details of EXAFS Fit Parameters of Tc-99 Adsorbed to and Coprecipitated with Magnetite and Subsequent Air Oxidation in the Intermediate Cement Leachate (pH 12.5)[a]

sample	Tc-	CN	$R + \Delta R$ (Å)	σ^2 (Å^2)	ΔE_0 (eV)	$S0^2$	X_v^2	R
ICL sorption	O	6[c]	2.02 (1)	0.004 (0)	−1.5 ± 1.4	0.90[c]	116.1	0.025
	Tc	6[c]	3.28 (3)	0.016 (3)				
ICL coppt, reduced	O	6[c]	2.00 (1)	0.005 (1)	−5.0 ± 1.6	0.90[c]	317.2	0.024
	Fe_1	4.3 ± 1.5	3.04 (2)	0.008 (3)[d]				
	Fe_2	4.0 ± 1.4	3.48 (2)	0.008 (3)[d]				
	O_{MS}[b]	6[c]	4.00 (2)	0.010 (1)				
ICL coppt, oxidized	O	6[c]	1.99 (1)	0.004 (1)	−4.7 ± 1.5	0.90[c]	185.5	0.026
21 days	Fe_1	4.3 ± 1.2	3.05 (1)	0.007 (2)[d]				
	Fe_2	3.6 ± 1.1	3.47 (2)	0.007 (2)[d]				
	O_{MS}[b]	6[c]	3.99 (2)	0.008 (1)				
ICL coppt, oxidized	O	6[c]	1.99 (1)	0.004 (1)	−5.0 ± 1.7	0.90[c]	549.0	0.027
152 days	Fe_1	4.4 ± 1.3	3.04 (1)	0.006 (2)[d]				
	Fe_2	3.7 ± 1.2	3.47 (2)	0.006 (2)[d]				
	O_{MS}[b]	6[c]	3.98 (2)	0.008 (1)				
magnetite[69]	O	6	2.06					
	Fe_1	6	2.97					
	Fe_2	6	3.48					

[a]CN denotes coordination number; $R + \Delta R$ denotes atomic distance; σ^2 denotes Debye−Waller factor; ΔE_0 denotes the shift in energy from the calculated Fermi level; $S0^2$ denotes the amplitude factor; X_v^2 denotes the reduced Chi square value; R denotes the "goodness of fit" factor; the subscript MS denotes multiple scattering paths. Numbers in parentheses are 1 standard deviation on the last decimal place. [b]The multiple scattering paths considered were linear paths, and their ΔR and σ^2 parameters were evaluated as multiples of the corresponding single scattering path parameter. [c]Parameter was fixed. [d]Parameters were tied in a given fit.

The ionic radii of Tc(IV) and Fe(III) are identical at 0.785 Å,[71] and so, the octahedrally coordinated site in the magnetite structure should accommodate Tc(IV) with little distortion. There is an excess charge associated with Tc(IV) substituting for octahedrally coordinated Fe(III), and this may cause the slightly lengthened Tc−Fe_1 atomic distance (~3.05 Å) observed from the EXAFS fitting in our samples compared to the Fe−Fe distance in magnetite (2.97 Å). The excess charge associated with the Tc(IV) substitution must be balanced through charge compensation.[39] One suitable mechanism to do this would be for coupled substitution of a lower charged ion, but no credible candidate exists in our system. Alternatively, the solid may compensate the charge through creation of a vacancy site or through reduction of Fe(III) to Fe(II) as in the case of Ti(IV) substitution into magnetite,[72] and this is the most likely mechanism here, although the relatively low concentration of Tc-99 in the samples at 0.1 wt % means that direct evidence for this was not available in our systems. Although there is no indication of the presence of a surface Tc(IV) phase in the EXAFS or the dissolution data, destructive interference between potential Tc−Tc and Tc−Fe signals has been reported[40,73] and we cannot definitively rule out minor contributions from a surface Tc(IV) phase in the reduced coprecipitated sample.

Tc(IV) Retention during Oxidation. Comparison of the spectra from the two oxidized samples and their respective fits to the reduced coprecipitation sample revealed that oxidation of Fe(II) to Fe(III), as confirmed from XRD measurements, had no significant effect on the speciation of the Tc-99 remaining in the solid even though significant maghematization and oxidation to goethite had occurred by 152 days. Indeed, in the 152 day sample, Tc-99 remained as Tc(IV) and could be

modeled as being predominantly substituted for Fe(III) in octahedral sites within the magnetite/maghemite structure. The presence of significant (~50%) goethite has little effect on the Tc EXAFS in these systems. Interestingly, the fits to the 21 and 152 day oxidized samples do not perfectly capture features in the EXAFS in the k = 10−12 Å^{-1} range (Figures 4 and SI-6, Supporting Information) which become more apparent with greater oxidation of the samples. Addition of a Tc−Fe distance that could be indicative of Tc(IV) incorporation into a secondary goethite phase (~3.2 Å) returned physically unrealistic Debye−Waller Factors, and so, this model was discounted. Changes in the host mineral structure could account for these features, for example, creation of vacancies during maghematization, but such effects were challenging to reproduce within the EXAFS model.

Our dissolution data suggest that a Tc-99 poor layer was created in the magnetite upon oxidation, and 1 M HCl extractions suggest ~10 wt % of the particle volume is depleted in Tc. Formation of trace element depleted surface layers following oxidation has previously been observed for a range of trace-metal incorporated magnetites.[66] Comparison with this past work suggests that this depleted layer forms due to a mix of oxidative Tc-99 diffusion out of the solid into solution and outward diffusion of Fe during dynamic maghematization.[45,66] The Fe(II)/Fe(III) ratio in solids dropped from 0.5 to between 0.12−0.21 in the ICL and OCL oxidation experiments indicating that at least ~40% of the magnetite had been oxidized to maghemite. This equates to a surface layer with a thickness of ~15% of the particle radius. This indicates that a model where there are three "zones" in a cross-section through the oxidized particles, an outer maghemite layer with essentially no Tc-99 (~10%), a maghemite layer containing Tc-99 (~30%), and a magnetite core containing Tc-99 (~60%), could explain the Tc distribution in the samples. This three layer model is an oversimplification of the true system since there will not be a discrete boundary between magnetite and maghemite.[46] However, it is clear that, despite significant oxidation of the magnetite, solid associated Tc(IV) remains in the reduced state and resides in regions with complete oxidation of structural Fe(II) to Fe(III) and in a site almost identical to the octahedral site in magnetite (Figure 4, Table 2). This suggests that a significant fraction of Tc(IV) incorporated into iron oxides may be recalcitrant to oxidation even if the iron oxide itself is oxidized, with the suggestion that irreversible binding of Tc-99 is possible in these systems.

It has recently been demonstrated that secondary armoring of Tc(IV) incorporated into goethite crystals protects the Tc(IV) from oxidation and decreases the release of Tc-99 from within goethite.[37,38] In our systems, it is possible that the maghematization process resulted in armoring of the Tc(IV) incorporated magnetite through creation of an Fe(III)-rich rind via outward diffusion of Fe(III).[45] Such a rind could serve to limit or even prevent further outward diffusion of Tc-99 to solution, which may account for the observation that, on reoxidation of magnetite, Tc-99 release to solution was restricted and was essentially at steady state after the initial rapid release during the first couple of weeks of oxidation. This suggests that Tc(IV) incorporated into magnetite may be stable over an extended time, even in the event of a shift to oxidizing conditions, and implies that reductively scavenged Tc-99 may be essentially irreversibly bound within magnetite over a wide range of geochemical conditions.

Effect of Solution pH. The EXAFS spectra for all of the coprecipitation samples were broadly similar for each of the three leachates (Figure SI-6 and Table SI-5, Supporting Information). This suggests that the behavior of Tc-99 during magnetite crystallization was pH independent, perhaps unsurprising given the predicted speciation of Tc in solution as TcO_4^- over the entire pH range (10.5−13.1).[9] The YCL (pH 13.1) and OCL (pH 10.5) fits were the same as the ICL (pH 12.5) fits; the reduced coprecipitation sample data were again best fit with the model of Tc(IV) incorporation into the magnetite octahedral site, as were the data from the oxidized samples. From the analysis of the XRD patterns, up to 20% of goethite crystallized in the YCL (pH 13.1) and ICL (pH 12.5) reduced systems. This however had no measurable impact on the Tc-99 speciation evidenced by the similarity of the EXAFS spectra and best fits to the pure magnetite OCL (pH 10.5) system. The coordination of Fe(III) in goethite is similar to that of Fe(III) in an octahedral site in magnetite: Fe(III) is octahedrally coordinated by O at ~2 Å, and there are shells of Fe at ~3 and ~3.5 Å with coordination of 2 and 4, respectively; however, there is an additional pair of Fe atoms at ~3.3 Å.[74] The total Fe−Fe coordination in goethite of 8 matches the total Tc−Fe coordination in our incorporated iron oxides. This necessitated examination of the possibility that Tc-99 resided in the goethite. Despite recent evidence of Tc(IV) incorporation into goethite,[37,38] our data could not be fitted using the published model from this work[37,38] and clearly show a coordination environment where Tc-99 was best modeled by incorporation into magnetite/maghemite. However, we cannot rule out the possibility that a small fraction of Tc-99 is residing in goethite present in the YCL (pH 13.1), ICL (pH 12.5), and 152 day oxidized OCL (pH 10.5) systems.

Implications for Tc-99 Behavior in the Environment. The data presented show that Tc(VII) is reduced to Tc(IV) and incorporated into the magnetite structure during crystallization from a ferrihydrite precursor, with 60−70% of the incorporated Tc(IV) retained as Tc(IV) during relatively robust, long-term reoxidation. Counterintuitively, the oxidation process may in fact aid retention of a sizable proportion of Tc(IV) within the magnetite/maghemite via an armoring process with Fe(III), leaving a significant fraction of the Tc(IV) recalcitrant to oxidation. Incorporation of Tc-99 into magnetite may offer a long-term sequestration mechanism for significant quantities of Tc-99 in alkaline environments (pH >10) where magnetite is present and may help to explain previously observed recalcitrance of Tc-99 during reoxidation of reduced, iron oxide-bearing sediments. It is noteworthy that additional geochemical variables not considered in this study, e.g., groundwater chemistry, may have significant impacts on the ability of iron oxides to sequester Tc-99 and merit further investigation. For example, the presence of silica has been shown to inhibit ferrihydrite crystallization to goethite and hematite,[75] although it does not seem to affect magnetite crystallization at circum-neutral pH.[76]

Given that Tc(VII) was reduced and incorporated into magnetite over the entire experimental pH range and that magnetite has been shown to be a significant component in the corrosion of iron and steel under anaerobic conditions,[77] this study highlights the potential for significant retention of Tc-99 in radioactive waste disposal as a consequence of waste from iron corrosion. The mechanism of Tc(VII) reductive immobilization and incorporation to magnetite could therefore

present a significant sink for Tc(VII) in both waste disposal and contaminated land scenarios.

■ ASSOCIATED CONTENT

Supporting Information

Supporting Information includes additional figures and data tables for TEM/XAS analysis. This material is available free of charge via the Internet at http://pubs.acs.org.

■ AUTHOR INFORMATION

Corresponding Author

*E-mail: katherine.morris@manchester.ac.uk.

Notes

The authors declare no competing financial interest.

■ ACKNOWLEDGMENTS

This work has been funded as part of the UK Natural Environment Research Council (NERC) BIGRAD consortium through consortium grant NE/H007768/1. Diamond Light Source Beamtime grants SP8070, SP8544 and SP8941. We thank Carolyn Pearce for helpful discussion, Richard Doull for assistance at Diamond, Dr. Mike Ward and Dr. Andy Brown for assistance with TEM, and Dr. John Waters for XRD analyses.

■ REFERENCES

(1) Boyd, G. E. Osmotic and Activity Coefficients of Aqueous $NaTcO_4$ and $NaReO_4$ Solutions at 25°C. *J. Solution Chem.* **1978**, *7*, 229−238.

(2) Eriksen, T. E.; Ndalamba, P.; Bruno, J.; Caceci, M. The Solubility of $TcO_2{\cdot}nH_2O$ in Neutral to Alkaline Solutions Under Constant pCO_2. *Radiochim. Acta* **1992**, *58*−*59*, 67−70.

(3) Kunze, S.; Neck, V.; Gompper, K.; Fanghänel, T. Studies on the Immobilization of Technetium Under Near Field Geochemical Conditions. *Radiochim. Acta* **1996**, *74*, 159−163.

(4) Baston, G. M. N.; De Canniere, P. R.; Ilett, D. J.; Cowper, M. M.; Pilkington, N. J.; Tweed, C. J.; Wang, L.; Williams, S. J. Technetium Behaviour in Boom Clay - A Laboratory and Field Study. *Radiochim. Acta* **2002**, *90*, 735−740.

(5) Lear, G.; McBeth, J. M.; Boothman, C.; Gunning, D. J.; Ellis, B. L. B. L.; Lawson, R. S.; Morris, K.; Burke, I. T.; Bryan, N. D.; Brown, A. P.; et al. Probing the Biogeochemical Behavior of Technetium Using a Novel Nuclear Imaging Approach. *Environ. Sci. Technol.* **2010**, *44*, 156−162.

(6) Burke, I. T.; Livens, F. R.; Lloyd, J. R.; Brown, A. P.; Law, G. T. W.; McBeth, J. M.; Ellis, B. L.; Lawson, R. S.; Morris, K. The Fate of Technetium in Reduced Estuarine Sediments: Combining Direct and Indirect Analyses. *Appl. Geochem.* **2010**, *25*, 233−241.

(7) Corkhill, C. L.; Bridge, J. W.; Chen, X. C.; Hillel, P.; Thornton, S. F.; Romero-Gonzalez, M. E.; Banwart, S. A.; Hyatt, N. C. Real-Time Gamma Imaging of Technetium Transport Through Natural and Engineered Porous Materials for Radioactive Waste Disposal. *Environ. Sci. Technol.* **2013**, *47*, 13857−13864.

(8) Hallam, R. J.; Evans, N. D. M.; Jain, S. L. Sorption of Tc(IV) to Some Geological Materials with Reference to Radioactive Waste Disposal. *Mineral. Mag.* **2011**, *75*, 2439−2448.

(9) Icenhower, J. P.; Qafoku, N. P.; Zachara, J. M.; Martin, W. J. The Biogeochemistry of Technetium: A Review of the Behavior of an Artificial Element in the Natural Environment. *Am. J. Sci.* **2011**, *310*, 721−752.

(10) Sellafield Ltd. *Monitoring our Environment - Discharges and Monitoring in the United Kingdom Annual Report 2012*; Nuclear Decommissioning Authority: Cumbria, UK, 2012; p 71.

(11) Thorpe, C. L.; Boothman, C.; Lloyd, J. R.; Law, G. T. W.; Bryan, N. D.; Atherton, N.; Livens, F. R.; Morris, K. The Interactions of Strontium and Technetium with Fe(II) Bearing Biominerals: Implications for Bioremediation of Radioactively Contaminated Land. *Appl. Geochem.* **2014**, *40*, 135−143.

(12) McBeth, J. M.; Lear, G.; Lloyd, J. R.; Livens, F. R.; Morris, K.; Burke, I. T. Technetium Reduction and Reoxidation in Aquifer Sediments. *Geomicrobiol. J.* **2007**, *24*, 189−197.

(13) Lukens, W. W.; Shuh, D. K.; Schroeder, N. C.; Ashley, K. R. Identification of the Non-Pertechnetate Species in Hanford Waste Tanks, Tc(I)-Carbonyl Complexes. *Environ. Sci. Technol.* **2004**, *38*, 229−233.

(14) Peretyazhko, T. S.; Zachara, J. M.; Kukkadapu, R. K.; Heald, S. M.; Kutnyakov, I. V.; Resch, C. T.; Arey, B. W.; Wang, C. M.; Kovarik, L.; Phillips, J. L.; et al. Pertechnetate (TcO_4^-) Reduction by Reactive Ferrous Iron Forms in Naturally Anoxic, Redox Transition Zone Sediments from the Hanford Site, USA. *Geochim. Cosmochim. Acta* **2012**, *92*, 48−66.

(15) Aarkrog, A.; Chen, Q.; Dahlgaard, H.; Nielsen, S. P.; Trapeznikov, A.; Pozolotina, V. Evidence of Tc-99 in Ural River Sediments. *J. Environ. Radioact.* **1997**, *37*, 201−213.

(16) Farrell, J.; Bostick, W. D.; Jarabek, R. J.; Fiedor, J. N. Electrosorption and Reduction of Pertechnetate by Anodically Polarized Magnetite. *Environ. Sci. Technol.* **1999**, *33*, 1244−1249.

(17) Peretyazhko, T.; Zachara, J. M.; Heald, S. M.; Jeon, B.-H.; Kukkadapu, R. K.; Liu, C.; Moore, D.; Resch, C. T. Heterogeneous Reduction of Tc(VII) by Fe(II) at the Solid−Water Interface. *Geochim. Cosmochim. Acta* **2009**, *72*, 1521−1539.

(18) Pearce, C. I.; Liu, J.; Baer, D. R.; Qafoku, O.; Heald, S. M.; Arenholz, E.; Grosz, A. E.; McKinley, J. P.; Resch, C. T.; Bowden, M. E.; et al. Characterization of Natural Titanomagnetites ($Fe_{3-x}Ti_xO_4$) for Studying Heterogeneous Electron Transfer to Tc(VII) in the Hanford Subsurface. *Geochim. Cosmochim. Acta* **2014**, *128*, 114−127.

(19) Wharton, M. J.; Atkins, B.; Charnock, J. M.; Livens, F. R.; Pattrick, R. A. D.; Collison, D. An X-Ray Absorption Spectroscopy Study of the Coprecipitation of Tc and Re with Mackinawite (FeS). *Appl. Geochem.* **2000**, *15*, 347−354.

(20) Fan, D.; Anitori, R. P.; Tebo, B. M.; Tratnyek, P. G.; Lezama Pacheco, J. S.; Kukkadapu, R. K.; Engelhard, M. H.; Bowden, M. E.; Kovarik, L.; Arey, B. W. Reductive Sequestration of Pertechnetate ($^{99}TcO_4^-$) by Nano Zerovalent Iron (nZVI) Transformed by Abiotic Sulfide. *Environ. Sci. Technol.* **2013**, *47*, 5302−5310.

(21) Fan, D.; Anitori, R. P.; Tebo, B. M.; Tratnyek, P. G.; Lezama Pacheco, J. S.; Kukkadapu, R. K.; Kovarik, L.; Engelhard, M. H.; Bowden, M. E. Oxidative Remobilization of Technetium Sequestered by Sulfide-Transformed Nano Zerovalent Iron. *Environ. Sci. Technol.* **2014**, *48*, 7409−7417.

(22) Zachara, J. M.; Heald, S. M.; Jeon, B.-H.; Kukkadapu, R. K.; Liu, C.; McKinley, J. P.; Dohnalkova, A. C.; Moore, D. A. Reduction of Pertechnetate [Tc(VII)] by Aqueous Fe(II) and the Nature of Solid Phase Redox Products. *Geochim. Cosmochim. Acta* **2007**, *71*, 2137−2157.

(23) Peretyazhko, T.; Zachara, J. M.; Heald, S. M.; Kukkadapu, R. K.; Liu, C.; Plymale, A. E.; Resch, C. T. Reduction of Tc(VII) by Fe(II) Sorbed on Al (Hydr)Oxides. *Environ. Sci. Technol.* **2008**, *42*, 5499−5506.

(24) Lloyd, J. R.; Sole, V. A.; Van Praagh, C. V. G.; Lovley, D. R. Direct and Fe(II)-Mediated Reduction of Technetium by Fe(III)-Reducing Bacteria. *Appl. Environ. Microbiol.* **2000**, *66*, 3743−3749.

(25) Burke, I. T.; Boothman, C.; Lloyd, J. R.; Mortimer, R. J. G.; Livens, F. R.; Morris, K. Effects of Progressive Anoxia on the Solubility of Technetium in Sediments. *Environ. Sci. Technol.* **2005**, *39*, 4109−4116.

(26) McBeth, J. M.; Lloyd, J. R.; Law, G. T. W.; Livens, F. R.; Burke, I. T.; Morris, K. Redox Interactions of Technetium with Iron-Bearing Minerals. *Mineral. Mag.* **2011**, *75*, 2419−2430.

(27) Cui, D.; Eriksen, T. E. Reduction of Pertechnetate by Ferrous Iron in Solution: Influence of Sorbed and Precipitated Fe(II). *Environ. Sci. Technol.* **1996**, *30*, 2259−2262.

(28) Walton, F. B.; Paquette, J.; Ross, J. P. M.; Lawrence, W. E. Tc(IV) and Tc(VII) Interactions with Iron Oxides. *Nucl. Chem. Waste Manage.* **1986**, *6*, 121−126.

(29) Cui, D.; Eriksen, T. E. Reduction of Pertechnetate in Solution by Heterogeneous Electron Transfer from Fe(II)-Containing Geological Material. *Environ. Sci. Technol.* **1996**, *30*, 2263−2269.
(30) Lee, J.-H.; Zachara, J. M.; Fredrickson, J. K.; Heald, S. M.; McKinley, J. P.; Plymale, A. E.; Resch, C. T.; Moore, D. A. Fe(II)- and Sulfide-Facilitated Reduction of $^{99}Tc(VII)O_4^-$ in Microbially Reduced Hyporheic Zone Sediments. *Geochim. Cosmochim. Acta* **2014**, *136*, 247−264.
(31) Morris, K.; Butterworth, J. C.; Livens, F. R. Evidence for the Remobilization of Sellafield Waste Radionuclides in an Intertidal Salt Marsh, West Cumbria, UK. *Estuarine, Coastal Shelf Sci.* **2000**, *51*, 613−625.
(32) Morris, K.; Livens, F. R.; Charnock, J. M.; Burke, I. T.; McBeth, J. M.; Begg, J. D. C.; Boothman, C.; Lloyd, J. R. An X-Ray Absorption Study of the Fate of Technetium in Reduced and Reoxidised Sediments and Mineral Phases. *Appl. Geochem.* **2008**, *23*, 603−617.
(33) Burke, I. T.; Boothman, C.; Lloyd, J. R.; Livens, F. R.; Charnock, J. M.; McBeth, J. M.; Mortimer, R. J. G.; Morris, K. Reoxidation Behavior of Technetium, Iron, and Sulfur in Estuarine Sediments. *Environ. Sci. Technol.* **2006**, *40*, 3529−3535.
(34) Begg, J. D. C.; Burke, I. T.; Morris, K. The Behaviour of Technetium During Microbial Reduction in Amended Soils from Dounreay, UK. *Sci. Total Environ.* **2007**, *373*, 297−304.
(35) Geissler, A.; Law, G. T. W.; Boothman, C.; Morris, K.; Burke, I. T.; Livens, F. R.; Lloyd, J. R. Microbial Communities Associated with the Oxidation of Iron and Technetium in Bioreduced Sediments. *Geomicrobiol. J.* **2011**, *28*, 507−518.
(36) Begg, J. D. C.; Burke, I. T.; Charnock, J. M.; Morris, K. Technetium Reduction and Reoxidation Behaviour in Dounreay Soils. *Radiochim. Acta* **2008**, *96*, 631−636.
(37) Um, W.; Chang, H.-S.; Icenhower, J. P.; Lukens, W. W.; Serne, R. J.; Qafoku, N. P.; Westsik, J. H., Jr.; Buck, E. C.; Smith, S. C. Immobilization of $^{99}Tc(VII)$ by Fe(II)-Goethite and Limited Reoxidation. *Environ. Sci. Technol.* **2011**, *45*, 4904−4913.
(38) Um, W.; Chang, H.; Icenhower, J. P.; Lukens, W. W.; Jeffrey Serne, R.; Qafoku, N.; Kukkadapu, R. K.; Westsik, J. H. Iron Oxide Waste Form for Stabilizing ^{99}Tc. *J. Nucl. Mater.* **2012**, *429*, 201−209.
(39) Skomurski, F. N.; Rosso, K. M.; Krupka, K. M.; McGrail, B. P. Technetium Incorporation into Hematite (alpha-Fe_2O_3). *Environ. Sci. Technol.* **2010**, *44*, 5855−5861.
(40) Heald, S. M.; Krupka, K. M.; Brown, C. F. Incorporation of Pertechnetate and Perrhenate into Corroded Steel Surfaces Studied by X-Ray Absorption Fine Structure Spectroscopy. *Radiochim. Acta* **2012**, *100*, 243−253.
(41) Kobayashi, T.; Scheinost, A. C.; Fellhauer, D.; Gaona, X.; Altmaier, M. Redox Behavior of Tc(VII)/Tc(IV) Under Various Reducing Conditions in 0.1 M NaCl Solutions. *Radiochim. Acta* **2013**, *101*, 323−332.
(42) Tronc, E.; Belleville, P.; Jolivet, J. P.; Livage, J. Transformation of Ferric Hydroxide into Spinel by Fe(II) Adsorption. *Langmuir* **1992**, *8*, 313−319.
(43) Hansel, C. M.; Benner, S. G.; Neiss, J.; Dohnalkova, A.; Kukkadapu, R. K.; Fendorf, S. Secondary Mineralization Pathways Induced by Dissimilatory Iron Reduction of Ferrihydrite Under Advective Flow. *Geochim. Cosmochim. Acta* **2003**, *67*, 2977−2992.
(44) Hansel, C. M.; Benner, S. G.; Fendorf, S. Competing Fe(II)-Induced Mineralization Pathways of Ferrihydrite. *Environ. Sci. Technol.* **2005**, *39*, 7147−7153.
(45) Sidhu, P. S.; Gilkes, R. J.; Posner, A. M. Mechanism of the Low Temperature Oxidation of Synthetic Magnetites. *J. Inorg. Nucl. Chem.* **1977**, *39*, 1953−1958.
(46) Tang, J.; Myers, M.; Bosnick, K. A.; Brus, L. E. Magnetite Fe_3O_4 Nanocrystals: Spectroscopic Observation of Aqueous Oxidation Kinetics. *J. Phys. Chem. B* **2003**, *107*, 7501−7506.
(47) Gorski, C. A.; Nurmi, J. T.; Tratnyek, P. G.; Hofstetter, T. B.; Scherer, M. M. Redox Behavior of Magnetite: Implications for Contaminant Reduction. *Environ. Sci. Technol.* **2010**, *44*, 55−60.
(48) Berner, U. R. Evolution of Pore Water Chemistry During Degradation of Cement in a Radioactive Waste Repository Environment. *Waste Manage.* **1992**, *12*, 201−219.
(49) Wallace, S. H.; Shaw, S.; Morris, K.; Small, J. S.; Fuller, A. J.; Burke, I. T. Effect of Groundwater pH and Ionic Strength on Strontium Sorption in Aquifer Sediments: Implications for ^{90}Sr Mobility at Contaminated Nuclear Sites. *Appl. Geochem.* **2012**, *27*, 1482−1491.
(50) Wallace, S. H.; Shaw, S.; Morris, K.; Small, J. S.; Burke, I. T. Alteration of Sediments by Hyperalkaline K-Rich Cement Leachate: Implications for Strontium Adsorption and Incorporation. *Environ. Sci. Technol.* **2013**, *47*, 3694−3700.
(51) Lukens, W. W.; Bucher, J. I. J.; Edelstein, N. M.; Shuh, D. K. Products of Pertechnetate Radiolysis in Highly Alkaline Solution: Structure of $TcO_2{\cdot}xH_2O$. *Environ. Sci. Technol.* **2002**, *36*, 1124−1129.
(52) Fredrickson, J. K.; Zachara, J. M.; Plymale, A. E.; Heald, S. M.; McKinley, J. P.; Kennedy, D. W.; Liu, C. X.; Nachimuthu, P. Oxidative Dissolution Potential of Biogenic and Abiogenic TcO_2 in Subsurface Sediments. *Geochim. Cosmochim. Acta* **2009**, *73*, 2299−2313.
(53) Liu, J.; Pearce, C. I.; Qafoku, O.; Arenholz, E.; Heald, S. M.; Rosso, K. M. Tc(VII) Reduction Kinetics by Titanomagnetite ($Fe_{3-x}Ti_xO_4$) Nanoparticles. *Geochim. Cosmochim. Acta* **2012**, *92*, 67−81.
(54) Williamson, A. J.; Morris, K.; Shaw, S.; Byrne, J. M.; Boothman, C.; Lloyd, J. R. Microbial Reduction of Fe(III) Under Alkaline Conditions Relevant to Geological Disposal. *Appl. Environ. Microbiol.* **2013**, *79*, 3320−3326.
(55) Moyce, E. B. A.; Rochelle, C.; Morris, K.; Milodowski, A. E.; Chen, X.; Thornton, S.; Small, J. S.; Shaw, S. Rock Alteration in Alkaline Cement Waters over 15 Years and Its Relevance to the Geological Disposal of Nuclear Waste. *Appl. Geochem.* **2014**, DOI: 10.1016/j.apgeochem.2014.08.003.
(56) Cornell, R. M.; Schwertmann, U. *The Iron Oxides: Structure, Properties, Reactions, Occurences and Uses*; 2nd ed.; Wiley-VCH: Weinham, 2003.
(57) Viollier, E.; Inglett, P. W.; Hunter, K.; Roychoudhury, A. N.; Van Cappellen, P. The Ferrozine Method Revisited: Fe(II)/Fe(III) Determination in Natural Waters. *Appl. Geochem.* **2000**, *15*, 785−790.
(58) Burke, I. T.; Mosselmans, J. F. W.; Shaw, S.; Peacock, C. L.; Benning, L. G.; Coker, V. S. Impact of the Diamond Light Source on Research in Earth and Environmental Sciences: Current Work and Future Perspectives. *Philos. Trans. R. Soc. A* **2014**, in press; http://rsta.royalsocietypublishing.org/site/misc/forthcoming-issues.xhtml.
(59) Dent, A. J.; Cibin, G.; Ramos, S.; Smith, A. D.; Scott, S. M.; Varandas, L.; Pearson, M. R.; Krumpa, N. A.; Jones, C. P.; Robbins, P. E. B18: A Core XAS Spectroscopy Beamline for Diamond. *J. Phys. Conf. Ser.* **2009**, *190*, 012039.
(60) Ravel, B.; Newville, M. Athena, Artemis, Hephaestus: Data Analysis for X-Ray Absorption Spectroscopy Using IFEFFIT. *J. Synchrotron Radiat.* **2005**, *12*, 537−541.
(61) He, Y. T.; Traina, S. J. Transformation of Magnetite to Goethite Under Alkaline pH Conditions. *Clay Miner.* **2007**, *42*, 13−19.
(62) Kim, W.; Suh, C.-Y.; Cho, S.-W.; Roh, K.-M.; Kwon, H.; Song, K.; Shon, I.-J. A New Method for the Identification and Quantification of Magnetite−Maghemite Mixture Using Conventional X-Ray Diffraction Technique. *Talanta* **2012**, *94*, 348−352.
(63) Gorski, C. A.; Scherer, M. M. Determination of Nanoparticulate Magnetite Stoichiometry by Mossbauer Spectroscopy, Acidic Dissolution, and Powder X-Ray Diffraction: A Critical Review. *Am. Mineral.* **2010**, *95*, 1017−1026.
(64) Deer, W. A.; Howie, R. A.; Zussman, J. *An Introduction to the Rock Forming Minerals*; 2nd ed.; Wiley: New York, 1992.
(65) Sidhu, P. S.; Gilkes, R. J.; Posner, A. M. The Synthesis and Some Properties of Co, Ni, Zn, Cu, Mn and Cd Substituted Magnetites. *J. Inorg. Nucl. Chem.* **1978**, *40*, 429−435.
(66) Sidhu, P. S.; Gilkes, R. J.; Posner, A. M. Behaviour of Co, Ni, Zn, Cu, Mn, and Cr in Magnetite During Alteration to Maghemite and Hematite. *Soil Sci. Soc. Am. J.* **1980**, *44*, 135−138.

(67) Hess, N. J.; Xia, Y. X.; Rai, D.; Conradson, S. D. Thermodynamic Model for the Solubility of $TcO_2 \cdot xH_2O$(am) in the Aqueous Tc(IV)-Na^+-Cl^--H^+-OH^--H_2O System. *J. Solution Chem.* **2004**, *33*, 199−226.
(68) Downward, L.; Booth, C. H.; Lukens, W. W.; Bridges, F. A Variation of the F-Test for Determining Statistical Relevance of Particular Parameters in EXAFS Fits. In *X-Ray Absorption Fine Structure-XAFS13*; Hedman, B., Painetta, P., Eds.; American Institute of Physics: Melville, NY, 2007; Vol. *882*, pp 129−131.
(69) Fleet, M. E. The Structure of Magnetite. *Acta Crystallogr., Sect. B: Struct. Sci.* **1981**, *2549*, 917−920.
(70) Suzuki, Y.; Kelly, S. D.; Kemner, K. M.; Banfield, J. F. Radionuclide Contamination - Nanometre-Size Products of Uranium Bioreduction. *Nature* **2002**, *419*, 134.
(71) Shannon, R. D. Revised Effective Ionic-Radii and Systematic Studies of Interatomic Distances in Halides and Chalcogenides. *Acta Crystallogr., Sect. A* **1976**, *32*, 751−767.
(72) Pearce, C. I.; Qafoku, O.; Liu, J.; Arenholz, E.; Heald, S. M.; Kukkadapu, R. K.; Gorski, C. A.; Henderson, C. M. B.; Rosso, K. M. Synthesis and Properties of Titanomagnetite ($Fe_{3-x}Ti_xO_4$) Nanoparticles: A Tunable Solid-State Fe(II/III) Redox System. *J. Colloid Interface Sci.* **2012**, *387*, 24−38.
(73) Heald, S. M.; Zachara, J. M.; Jeon, B. H.; McKinley, J. P.; Kukkadapu, R.; Moore, D. XAFS Study of the Chemical and Structural States of Technetium in Fe(III) Oxide Co-Precipitates. In *X-Ray Absorption Fine Structure-XAFS13*; Hedman, B., Painetta, P., Eds.; American Institute of Physics: Melville, NY, 2007; Vol. *882*, pp 173−175.
(74) Szytula, A.; Burewicz, A.; Dimitrij, Z.; Krasnick, S.; Rzany, H.; Todorovi, J.; Wanic, A.; Wolski, W.; Dimitrijvic, Z.; Krasnicki, S.; et al. Neutron Diffraction Studies of α-FeOOH. *Phys. Status Solidi* **1968**, *429*, 429−434.
(75) Cornell, R. M.; Giovanoli, R.; Schindler, P. W. Effect of Silicate Species on the Transformation of Ferrihydrite into Goethite and Hematite in Alkaline Media. *Clays Clay Miner.* **1987**, *35*, 21−28.
(76) Kukkadapu, R. K.; Zachara, J. M.; Fredrickson, J. K.; Kennedy, D. W. Biotransformation of Two-Line Silica-Ferrihydrite by a Dissimilatory Fe(III)-Reducing Bacterium: Formation of Carbonate Green Rust in the Presence of Phosphate. *Geochim. Cosmochim. Acta* **2004**, *68*, 2799−2814.
(77) Music, S.; Gotic, M.; Popovic, S. X-Ray Diffraction and Fourier-Transform Infrared-Analysis of the Rust Formed by Corosion of Steel in Aqueous-Solutions. *J. Mater. Sci.* **1993**, *28*, 5744−5752.

Supporting Information for:

Incorporation and retention of 99-Tc(IV) in magnetite under high pH conditions

Timothy A. Marshall,[†] Katherine Morris,[†] Gareth T.W. Law,[‡] J. Frederick W. Mosselmans,[§] Pieter Bots,[†] Stephen A. Parry,[§] and Samuel Shaw [†]*

† Research Centre for Radwaste Disposal and Williamson Research Centre for Molecular Environmental Science, School of Earth, Atmospheric and Environmental Sciences, The University of Manchester, Manchester, M13 9PL, UK.

‡ Centre for Radiochemistry Research and Research Centre for Radwaste Disposal, School of Chemistry, The University of Manchester, Manchester, M13 9PL, UK.

§ Diamond Light Source Ltd, Harwell Science and Innovation Campus, Didcot, Oxfordshire, OX11 0DE, UK.

* email: katherine.morris@manchester.ac.uk

Submitted to ES&T

Number of pages: 16;

Number of Figures: 6 (Figure SI-1 to Figure SI-6);

Number of Tables: 5 (Table SI-1 to Table SI-5);

Synthetic Cement Leachate Preparation.

Three synthetic cement leachates have been used to mimic groundwater compositions in and around an evolving cementitious geological disposal facility (GDF). These reflect the chemistry of the dominant buffering phases and represent the early-, intermediate- and late-stage post closure environment.[1,2]

Young Cement Leachate (YCL, pH 13.1). The young cement leachate (YCL) is dominated by potassium and sodium hydroxide (KOH and NaOH respectively) dissolution. The solution was prepared by first degassing 18 MΩ Milli-Q water with oxygen-free nitrogen (OFN) for 1 hour per liter before addition of the reagents. Whilst degassing and stirring the water with a magnetic stir bar, 5.2 gL^{-1} potassium hydroxide, 3.8 gL^{-1} sodium hydroxide and 0.1 gL^{-1} calcium hydroxide ($Ca(OH)_2$) were added. The solution was sealed and left on the stir plate for 24 hours, after which it was stored in an anaerobic chamber (5 % H_2, balance N_2, maintained at < 1 ppm O_2 and CO_2).

Intermediate Cement Leachate (ICL, pH 12.5). The intermediate cement leachate (ICL) is dominated by calcium hydroxide ($Ca(OH)_2$) dissolution. The solution was prepared by first degassing 18 MΩ Milli-Q water with oxygen-free nitrogen (OFN) for 1 hour per liter before addition of the reagent. Whilst degassing and stirring the water with a magnetic stir bar, 1.2 gL^{-1} calcium hydroxide ($Ca(OH)_2$) was added. The solution was sealed and left on the stir plate for 24 hours, after which it was stored in an anaerobic chamber (5 % H_2, balance N_2, maintained at < 1 ppm O_2 and CO_2).

Old Cement Leachate (OCL, pH 10.5). The old cement leachate (OCL) is dominated by calcium-silicate-hydrate (C-S-H) phase dissolution. The solution was prepared by first degassing 18 MΩ Milli-Q water with oxygen-free nitrogen (OFN) for 1 hour per liter before addition of the reagent. Whilst degassing and stirring the water with a magnetic stir bar, 15 mgL^{-1} calcium hydroxide ($Ca(OH)_2$) was added. Dissolved silica was not included in the OCL since PHREEQC modelling predicted solubility of silica in equilibrium with tobermorite-14Å to be low (0.03 mmol). Although silica has been shown to

have an inhibitory effect on the crystallization of ferrihydrite to goethite and hematite[3], this does not appear to be the case with crystallization to magnetite.[4] The solution was sealed and left on the stirrer plate for 24 hours, after which it was stored in an anaerobic chamber (5 % H_2, balance N_2, maintained at < 1 ppm O_2 and CO_2).

Tc-99 distribution profile in magnetite particles

Magnetite dissolves isotropically which allows insight into the distribution of Tc-99 within the magnetite particles to be gained by total digestion in 1 M HCl.[5,6] Digestions were performed on the samples from the OCL system because potential contributions from Tc-99 possibly incorporated into goethite could be discounted with certainty since XRD confirmed these to be fully magnetite. A mass of solid (< 0.1 g) was allowed to fully dissolve in 40 mL 1 M HCl in centrifuge tubes placed onto an end-over-end rotator at 30 rpm to ensure complete mixing. Solution samples were removed periodically and filtered using syringe-top filter units with 0.22 μm polyethersulfone (PES) membrane filters to remove any suspended particles. The resultant solution was analyzed for Tc-99 by LSC and for total Fe by the ferrozine method[7] until no further increase in the solution concentration of Fe was observed. At this point the solid was deemed to have completely dissolved and the experiment ended. The Tc-99 and Fe in solution data were normalized to the maximum solution concentrations and plotted as Tc-99 versus Fe, providing a concentration gradient of Tc-99 with Fe dissolution and providing insight into the Tc distribution in the solid.

The Tc-99 distribution in the oxidized magnetite particles revealed formation of a Tc-99 deficient layer equating to ~ 10 wt. % Fe. Since the observed size range of the magnetite particles is in the order of several nm to 10s of nm (Figure SI-3, Figure SI-4), a simple spherical particle may be assumed as a generalization. Therefore, 10 wt. % of the Fe is contained in a surface layer with a thickness of 3.5 % of the radius of the particle. In a 30 nm particle, this equates to a surface layer 0.5 nm thick which is approximately one unit cell.

X-ray diffraction patterns from all synthetic cement leachates

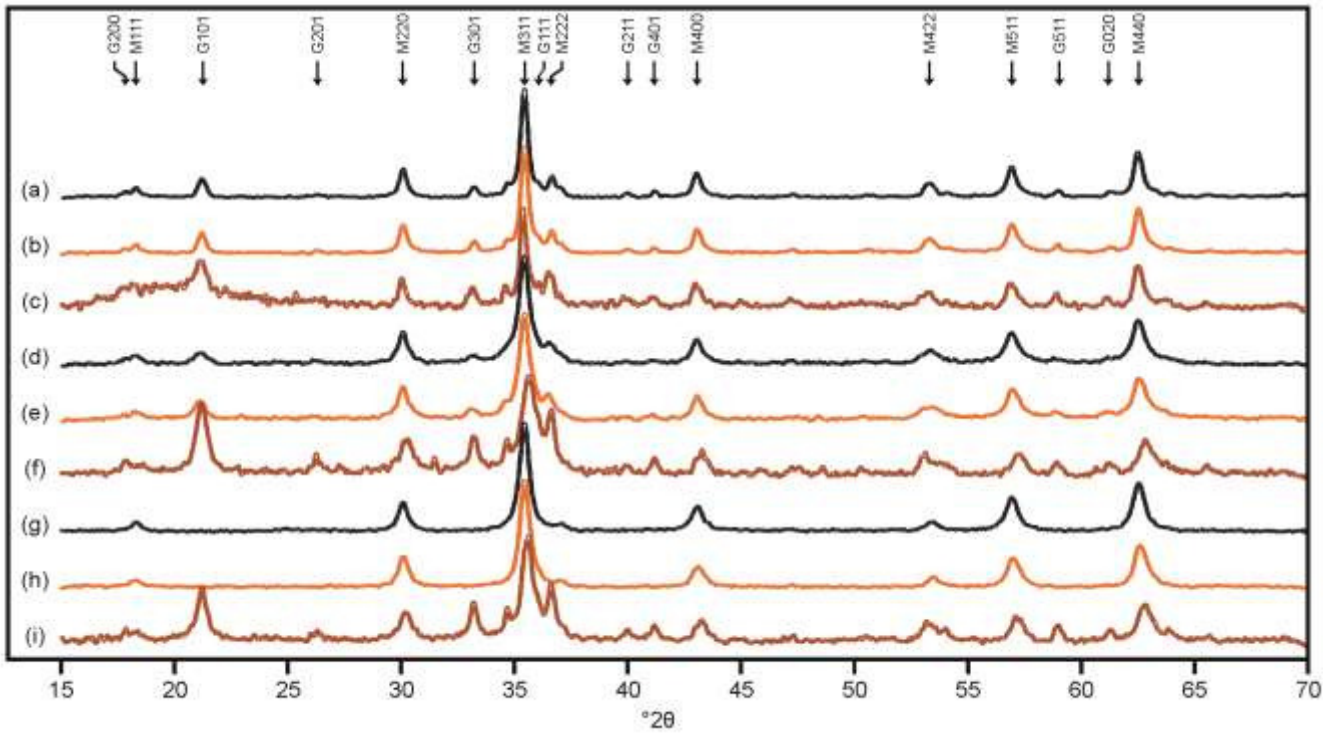

Figure SI-1 XRD patterns of reduced and air oxidized samples from each of the three synthetic cement leachates, YCL (pH 13.1), ICL (pH 12.5), and OCL (pH 10.5). (a) YCL reduced; (b) YCL 21 day oxidized; (c) YCL 152 day oxidized; (d) ICL reduced; (e) ICL 21 day oxidized; and (f) ICL 152 day oxidized; (g) OCL reduced; (h) OCL 21 day oxidized; and (i) OCL 152 day oxidized. Observable peaks are indexed, with M and G signifying magnetite and goethite, respectively.

Evidence of maghematisation from X-ray diffraction

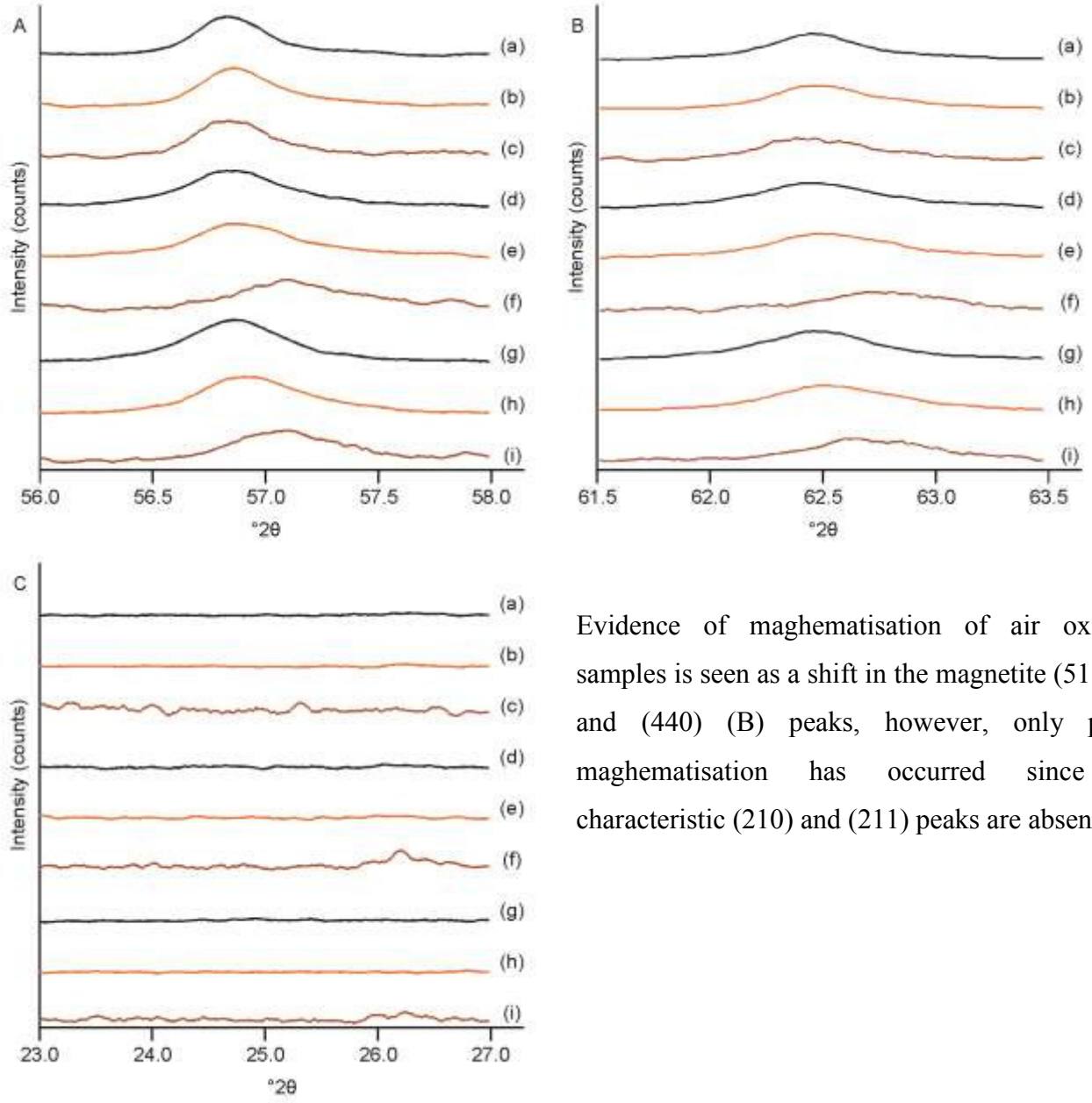

Evidence of maghematisation of air oxidized samples is seen as a shift in the magnetite (511) (A) and (440) (B) peaks, however, only partial maghematisation has occurred since the characteristic (210) and (211) peaks are absent (C).

Figure SI-2 Expanded XRD patterns of reduced and air oxidized samples from each of the three synthetic cement leachates, YCL (pH 13.1), ICL (pH 12.5), and OCL (pH 10.5). (a) YCL reduced; (b) YCL 21 day oxidized; (c) YCL 152 day oxidized; (d) ICL reduced; (e) ICL 21 day oxidized; and (f) ICL 152 day oxidized; (g) OCL reduced; (h) OCL 21 day oxidized; and (i) OCL 152 day oxidized.

TEM data from reduced magnetite

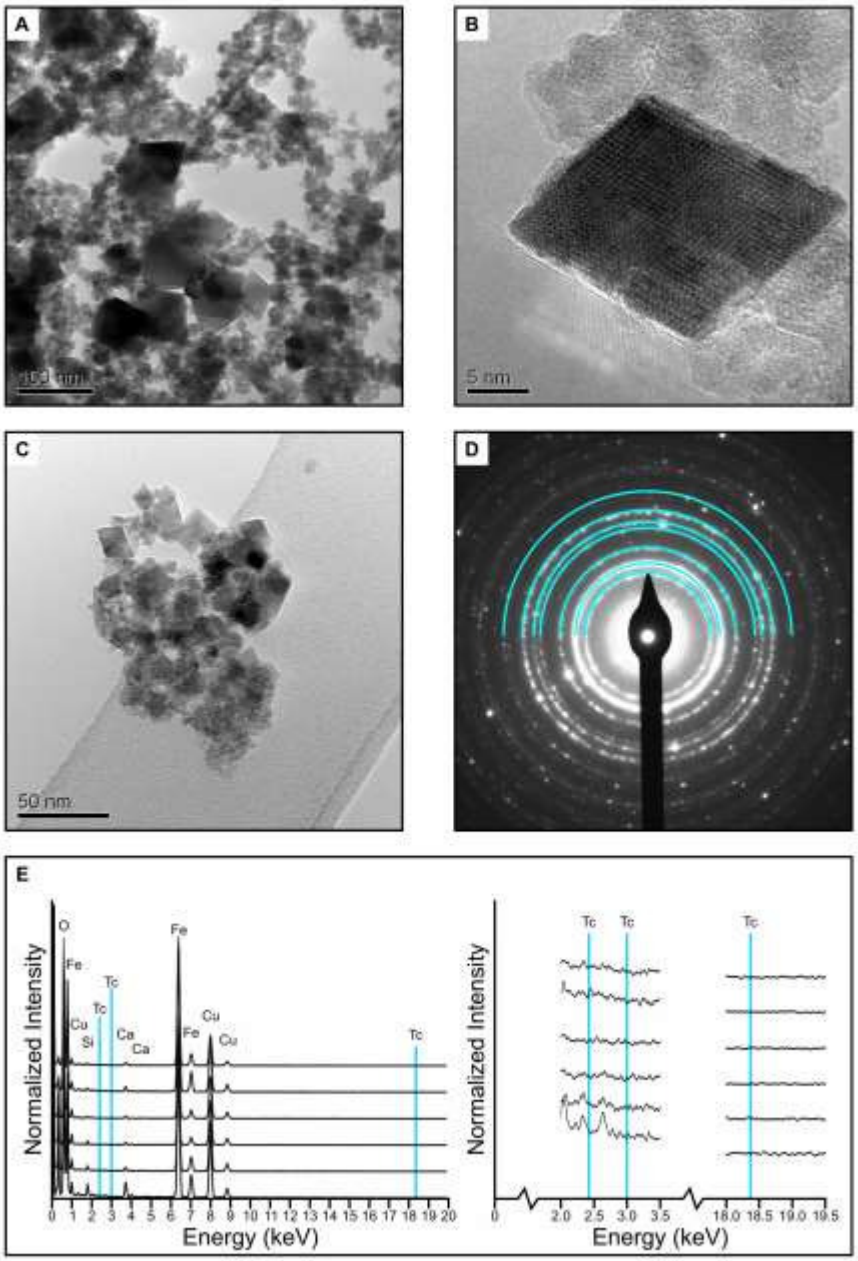

Figure SI-3 A-C – TEM images from reduced magnetite crystallised in ICL (pH 12.5); D – Selected area electron diffraction pattern from image C, with index for magnetite overlaying the pattern; E – stack of energy dispersive X-ray spectra taken from various magnetite clusters, with expanded sections on the right confirming the absence of Tc-99 peaks.

TEM data from oxidized magnetite

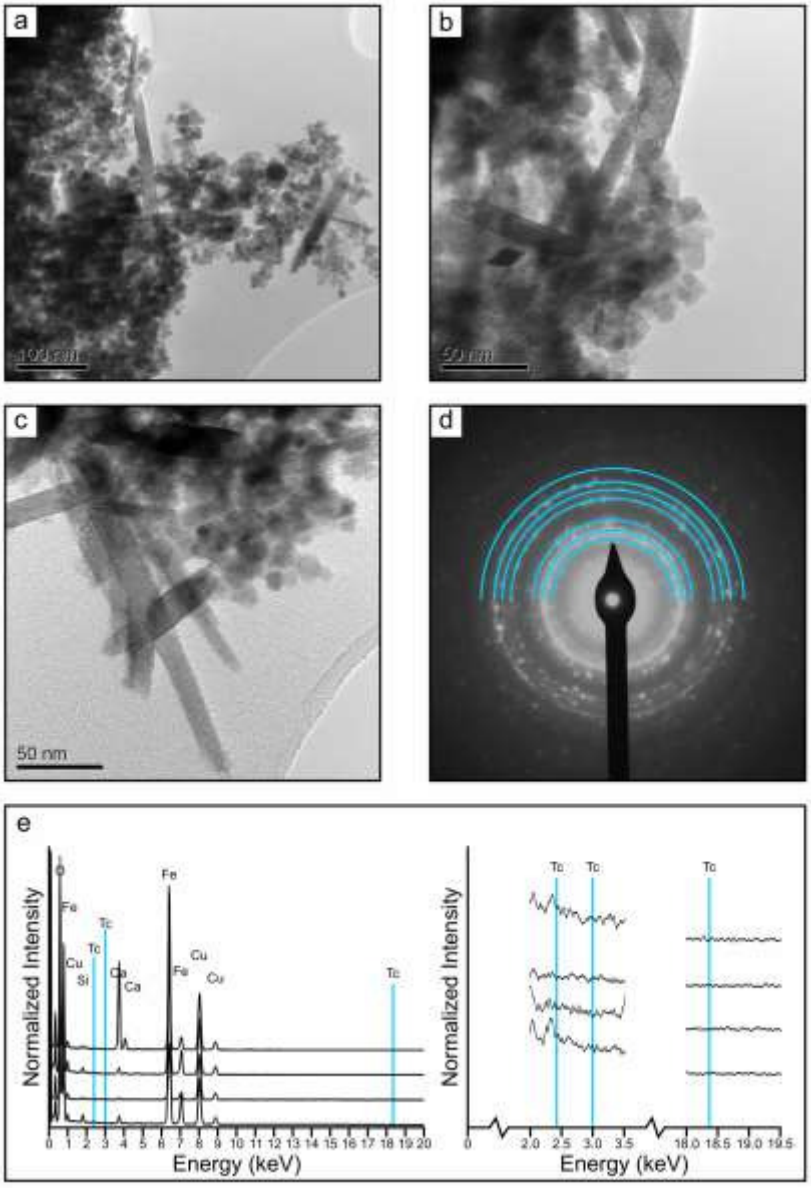

Figure SI-4 A - C – TEM images from oxidized magnetite crystallised in ICL (pH 12.5); D – Selected area electron diffraction pattern from image B, with index for maghemite overlaying the pattern; E – stack of energy dispersive X-ray spectra taken from various magnetite clusters, with expanded sections on the right confirming the absence of Tc-99 peaks.

XANES Linear Combination Fitting

Linear combination fitting was performed in Athena[8] on all XANES data collected from the sorption and coprecipitation experiments and in each of the three synthetic cement leachates. Two reference standards were used, the Tc(IV) reference being the $TcO_2 \cdot xH_2O$ reference from Hess et. al.[9] and a pertechnetate (Tc(VII), TcO_4^-) reference collected on the same beamtime as the experimental spectra. The fits were performed in normalized μ(E) space between -30 and +40 eV. Neither standard was stipulated as required in the fit but the weights of the standards were forced to between 0 and 1, and also to sum to 1. The results of the linear combination fitting are given in Table SI-1 below.

Table SI-1 Linear Combination Fitting Results for all XANES Spectra

Sample		R	X^2	X_v^2	Reference Weighting	
					TcO_2	TcO_4^-
YCL	Co-ppt reduced	0.009	0.148	2.09E-03	1.00 (0)	0.00 (0)
	Co-ppt oxidized 21 day	0.011	0.433	2.39E-03	1.00 (0)	0.00 (0)
	Co-ppt oxidized 152 day	0.012	0.177	2.49E-03	1.00 (0)	0.00 (0)
ICL	Sorption	0.009	0.386	2.13E-03	1.00 (0)	0.00 (0)
	Co-ppt reduced	0.009	0.146	2.02E-03	1.00 (0)	0.00 (0)
	Co-ppt oxidized 21 day	0.012	0.502	2.76E-03	1.00 (0)	0.00 (0)
	Co-ppt oxidized 152 day	0.011	0.172	2.43E-03	1.00 (0)	0.00 (0)
OCL	Co-ppt reduced	0.009	0.147	2.07E-03	1.00 (0)	0.00 (0)
	Co-ppt oxidized 21 day	0.012	0.504	2.78E-03	1.00 (0)	0.00 (0)
	Co-ppt oxidized 152 day	0.010	0.172	2.33E-03	1.00 (0)	0.00 (0)

R denotes the 'goodness of fit' factor; X^2 denotes the Chi square value; X_v^2 denotes the reduced Chi square value. Numbers in parentheses are standard deviation on the last decimal place

EXAFS fitting – ICL reduced sorption sample fits

The results of fits to the ICL sorption reduced data are presented below. The rationale behind fitting models (a)-(g) are given in Table SI-2. The fits are plotted in Figure SI-5 and coordination of the shells in each fit along with key fit metrics are given in Table SI-3. Results of F-test comparisons[10] are given in Table SI-4.

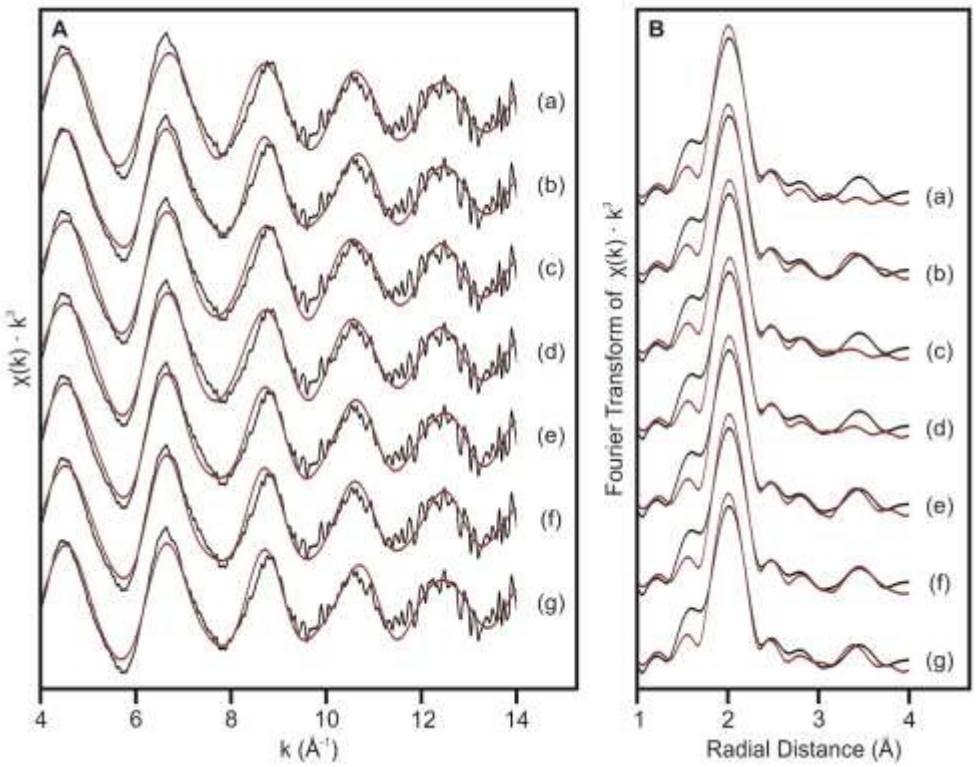

Figure SI-5 Technetium K-edge XAS spectra from Tc-99 adsorbed to magnetite in the intermediate stage cement leachate (ICL, pH 12.5) showing different fitting models outlined in Table SI-2. Panel A – k^3-weighted EXAFS; panel B – Fourier transform of k^3-weighted EXAFS, using a Hanning window function and plotted with phase shift calculated from Tc-O path. Black lines are data and red lines are fits to the data.

Table SI-2 Rationale of fitting models (a)-(g) applied to ICL sorption reduced data

Fit	Rationale
(a)	Tc(IV) octahedrally coordinated with a with a single shell of 6 O at ~2 Å
(b)	Disordered TcO_2 structure[11] modeled with a single shell of 6 Tc at ~3.3 Å in addition to 6 O at 2 Å
(c)	Monodentate adsorbed Tc(IV) species
(d)	Bidentate adsorbed Tc(VI) species
(e)	Monodentate adsorbed Tc(IV) species with Tc-Tc polymeric chain
(f)	Partial incorporation into magnetite
(g)	Polymeric Tc-Tc chain

Table SI-3 Coordination numbers for shells within the fitting models applied to the ICL reduced sorption data, as plotted in Figure SI-5 with key fit metrics for F-test comparison

Fit	(a)	(b)	(c)	(d)	(e)	(f)	(g)
Tc-O	6	6	6	6	6	6	6
Tc-Tc	-	6	-	-	1	-	2
Tc-Fe	-	-	-	-	-	1	-
Tc-Fe	-	-	1	2	1	1	-
df	2.6	13.3	13.3	13.3	11.3	11.3	13.3
X_v^2	418.2	96.8	189.1	199.8	165.7	167.2	138.1
R	0.027	0.030	0.046	0.048	0.036	0.036	0.039

Blank cell indicates shell was omitted from the fitting model; df denotes the degrees of freedom in the fit; X_v^2 denotes the reduced Chi square value; *R* denotes the 'goodness of fit' factor.

Table SI-4 F-test results from comparison of pairs of fits applied to ICL reduced sorption sample, as outlined in Table SI-2

F Test	α (%)	Comment
(a) vs (b)	0.1	Addition of a single shell of 6 Tc atoms at ~3.3 Å does not significantly improve the fit
(a) vs (c)	39.8	Monodentate adsorption does not significantly improve the fit
(a) vs (d)	47.4	Bidentate adsorption does not significantly improve the fit
(a) vs (e)	10.5	Monodentate adsorption of Tc-Tc chain does not significantly improve the fit
(a) vs (f)	10.7	Partial incorporation into magnetite does not significantly improve the fit
(a) vs (g)	15.6	Polymeric Tc-Tc chain does not significantly improve the fit

α denotes the probability that the two fits are statistically distinct from one another.

Full EXAFS dataset

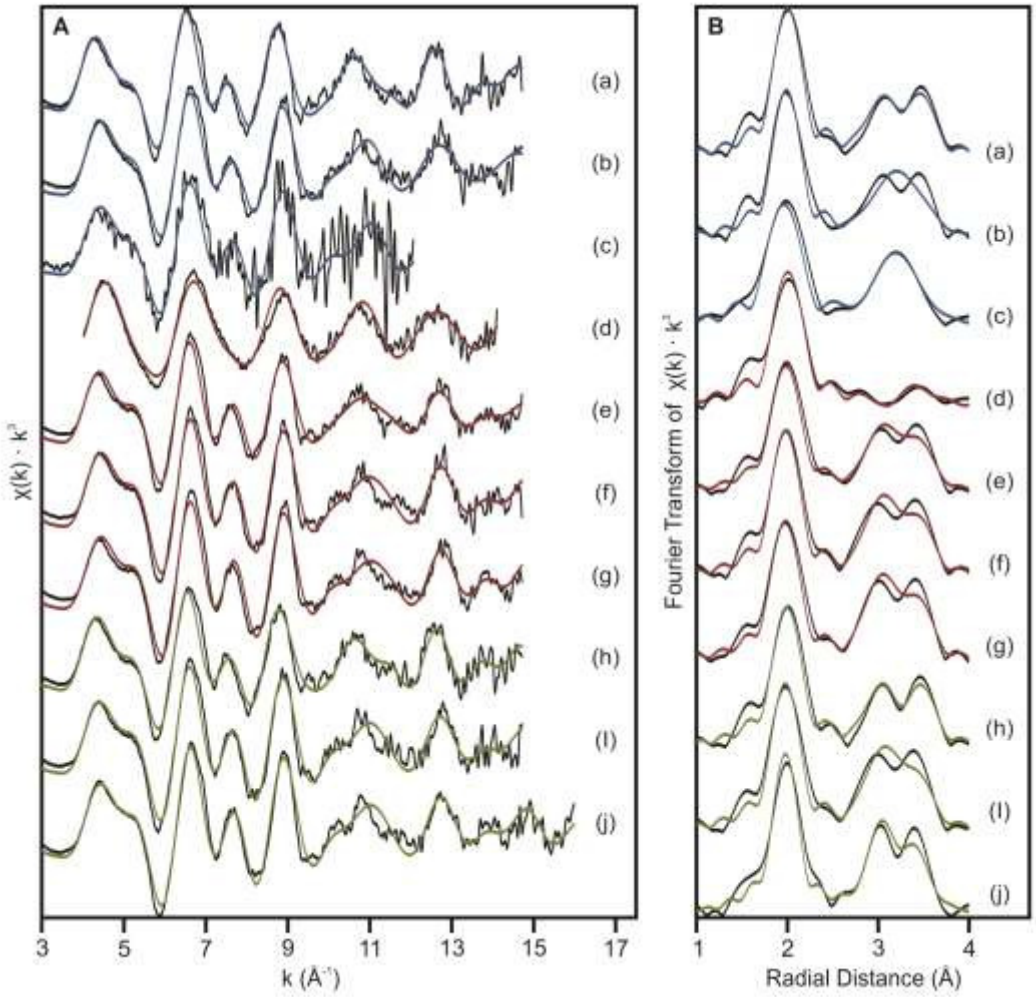

Figure SI-6 Technetium K-edge XAS spectra from Tc-99 adsorbed to, and coprecipitated with magnetite and subsequent air oxidation in all cement leachate experiments. Panel A – k^3-weighted EXAFS; panel B – Fourier transform of k^3-weighted EXAFS, using a Hanning window function and plotted with phase shift calculated from Tc-O path. Black lines are data and colored lines are fits to the data. (a) YCL coprecipitation reduced; (b) YCL coprecipitation oxidized 21 days; (c) YCL coprecipitation oxidized 152 days; (d) ICL adsorption reduced; (e) ICL coprecipitation reduced; (f) ICL coprecipitation oxidized 21 days; (g) ICL coprecipitation oxidized 152 days; (h) OCL coprecipitation reduced; (i) OCL coprecipitation oxidized 21 days; (j) OCL coprecipitation oxidized 152 days.

Table SI-5 Details of EXAFS fit parameters of Tc-99 adsorbed to, and coprecipitated with magnetite and subsequent air oxidation in all cement leachates, as presented in Figure SI-6. (a) YCL coprecipitation reduced; (b) YCL coprecipitation oxidized 21 days; (c) YCL coprecipitation oxidized 152 days; (d) ICL adsorption reduced; (e) ICL coprecipitation reduced; (f) ICL coprecipitation oxidized 21 days; (g) ICL coprecipitation oxidized 152 days; (h) OCL coprecipitation reduced; (i) OCL coprecipitation oxidized 21 days; (j) OCL coprecipitation oxidized 152 days.

		Tc-	CN	R (Å)	σ^2	ΔE_0	S_0^2	X_v^2	R
(a)	YCL co-ppt,	O	6[†]	2.02 (1)	0.004 (0)	-6.4 ± 1.0	0.90 [c]	102.9	0.018
	reduced	Fe_1	2.8 ± 0.7	3.06 (1)	0.006 (2)[‡]				
		Fe_2	3.5 ± 0.8	3.51 (1)	0.006 (2)[‡]				
		O_{MS} *	6[†]	4.04 (1)	0.007 (1)				
(b)	YCL co-ppt,	O	6[†]	2.00 (1)	0.004 (1)	-4.1 ± 1.5	0.90 [c]	129.2	0.029
	oxidized	Fe_1	6.0 ± 0.0	3.07 (1)	0.011 (1)[‡]				
	21 days	Fe_2	5.2 ± 1.6	3.47 (2)	0.011 (1)[‡]				
		O_{MS} *	6[†]	4.01 (2)	0.008 (1)				
(c)	YCL co-ppt,	O	6[†]	1.99 (1)	0.005 (1)	-7.4 ± 2.2	0.90 [c]	8.6	0.030
	oxidized	Fe_1	6.0 ± 0.0	3.06 (2)	0.011 (1)[‡]				
	152 days	Fe_2	6.0 ± 0.0	3.43 (3)	0.011 (1)[‡]				
		O_{MS} *	6[†]	3.97 (3)	0.009 (2)				
(d)	ICL sorption	O	6 [c]	2.02 (1)	0.004 (0)	-1.5 ± 1.4	0.90 [c]	116.1	0.025
		Tc	6 [c]	3.28 (3)	0.016 (3)				
(e)	ICL co-ppt,	O	6 [c]	2.00 (1)	0.005 (1)	-5.0 ± 1.6	0.90 [c]	317.2	0.024
	reduced	Fe_1	4.3 ± 1.5	3.04 (2)	0.008 (3) [‡]				
		Fe_2	4.0 ± 1.4	3.48 (2)	0.008 (3) [‡]				
		O_{MS} [b]	6 [c]	4.00 (2)	0.010 (1)				
(f)	ICL co-ppt,	O	6 [c]	1.99 (1)	0.004 (1)	-4.7 ± 1.5	0.90 [c]	185.5	0.026
	oxidized	Fe_1	4.3 ± 1.2	3.05 (1)	0.007 (2) [‡]				
	21 days	Fe_2	3.6 ± 1.1	3.47 (2)	0.007 (2) [‡]				
		O_{MS} [b]	6 [c]	3.99 (2)	0.008 (1)				

		Tc-	CN	R (Å)	σ^2	ΔE_0	S_0^2	X_v^2	R
(g)	ICL co-ppt,	O	6 [c]	1.99 (1)	0.004 (1)	-5.0 ± 1.7	0.90 [c]	549.0	0.027
	oxidized	Fe_1	4.4 ± 1.3	3.04 (1)	0.006 (2) ‡				
	152 days	Fe_2	3.7 ± 1.2	3.47 (2)	0.006 (2) ‡				
		O_{MS} [b]	6 [c]	3.98 (2)	0.008 (1)				
(h)	OCL co-ppt,	O	6†	2.01 (1)	0.004 (0)	-5.9 ± 1.1	0.90 [c]	99.7	0.019
	reduced	Fe_1	2.9 ± 0.7	3.05 (1)	0.006 (2)‡				
		Fe_2	3.4 ± 0.8	3.51 (1)	0.006 (2)‡				
		O_{MS} *	6†	4.02 (1)	0.008 (1)				
(i)	OCL co-ppt,	O	6†	1.99 (1)	0.004 (1)	-5.5 ± 1.5	0.90 [c]	161.7	0.024
	oxidized	Fe_1	4.8 ± 1.3	3.05 (1)	0.007 (2)‡				
	21 days	Fe_2	3.7 ± 1.2	3.47 (2)	0.007 (2)‡				
		O_{MS} *	6†	3.99 (2)	0.008 (1)				
(j)	OCL co-ppt,	O	6†	1.99 (1)	0.004 (0)	-4.9 ± 1.1	0.90 [c]	232.0	0.025
	oxidized	Fe_1	4.8 ± 1.1	3.05 (1)	0.007 (2)‡				
	152 days	Fe_2	3.7 ± 1.0	3.47 (2)	0.007 (2)‡				
		O_{MS} *	6†	3.98 (1)	0.008 (1)				

CN denotes coordination number; R denotes atomic distance; σ^2 denotes Debye-Waller factor; ΔE_0 denotes the shift in energy from the calculated Fermi level; S_0^2 denotes the amplitude factor; X_v^2 denotes the reduced Chi square value; *R* denotes the 'goodness of fit' factor; $_{MS}$ denotes multiple scattering paths. * the multiple scattering paths considered were linear paths and their ΔR and σ^2 parameters were evaluated as multiples of the corresponding single scattering path parameter. Numbers in parentheses are standard deviation on the last decimal place. ‡ denotes parameters were tied in a given fit. † denotes parameter was fixed.

The fits presented in Table SI-5 were constrained by tying the Debye Waller factors (DWF) of the two Fe shells. If this constraint was removed and all parameters were allowed to vary independently, the resultant fit was statistically indistinct from the constrained fit, yet physically unrealistic: the DWF for the outer Fe shell was half the DWF of the nearer shell (0.009 and 0.004 respectively) and coupled to this, the coordination of the outer shell decreased from ~4 to ~2.5. The coordination and DWF are correlated and so it is unsurprising to observe a decrease in both parameters, however, the refined values are physically unrealistic and hence justify imposing the constraint on Fe shell DWFs.

REFERENCES

(1) Berner, U. R. Evolution of Pore Water Chemistry During Degradation of Cement in a Radioactive Waste Repository Environment. *Waste Manag.* **1992**, *12*, 201–219.

(2) Moyce, E. B. A.; Rochelle, C.; Morris, K.; Milodowski, A. E.; Chen, X.; Thornton, S.; Small, J. S.; Shaw, S. Rock Alteration in Alkaline Cement Waters over 15 years and its Relevance to the Geological Disposal of Nuclear Waste. *Appl. Geochemistry* **2014**.

(3) Cornell, R. M.; Giovanoli, R.; Schindler, P. W. Effect of Silicate Species on the Transformation of Ferrihydrite into Goethite and Hematite in Alkaline Media. *Clays Clay Miner.* **1987**, *35*, 21–28.

(4) Kukkadapu, R. K.; Zachara, J. M.; Fredrickson, J. K.; Kennedy, D. W. Biotransformation of Two-Line Silica-Ferrihydrite by a Dissimilatory Fe(III)-Reducing Bacterium: Formation of Carbonate Green Rust in the Presence of Phosphate. *Geochim. Cosmochim. Acta* **2004**, *68*, 2799–2814.

(5) Sidhu, P. S.; Gilkes, R. J.; Posner, A. M. The Synthesis and Some Properties of Co, Ni, Zn, Cu, Mn and Cd Substituted Magnetites. *J. Inorg. Nucl. Chem.* **1978**, *40*, 429–435.

(6) Sidhu, P. S.; Gilkes, R. J.; Posner, A. M. Behaviour of Co, Ni, Zn, Cu, Mn, and Cr in Magnetite During Alteration to Maghemite and Hematite. *Soil Sci. Soc. Am. J.* **1980**, *44*, 135–138.

(7) Viollier, E.; Inglett, P. W.; Hunter, K.; Roychoudhury, A. N.; Van Cappellen, P. The Ferrozine Method Revisited: Fe(II)/Fe(III) Determination in Natural Waters. *Appl. Geochemistry* **2000**, *15*, 785–790.

(8) Ravel, B.; Newville, M. Athena, Artemis, Hephaestus: Data Analysis for X-Ray Absorption Spectroscopy Using IFEFFIT. *J. Synchrotron Radiat.* **2005**, *12*, 537–541.

(9) Hess, N. J.; Xia, Y. X.; Rai, D.; Conradson, S. D. Thermodynamic Model for the Solubility of $TcO_2 \cdot xH_2O$(am) in the Aqueous Tc(IV)-Na^+-Cl^--H^+-OH^--H_2O System. *J. Solution Chem.* **2004**, *33*, 199–226.

(10) Downward, L.; Booth, C. H.; Lukens, W. W.; Bridges, F. A Variation of the F-Test for Determining Statistical Relevance of Particular Parameters in EXAFS Fits. In *X-Ray Absorption Fine Structure-XAFS13*; Hedman, B.; Painetta, P., Eds.; 2007; Vol. 882, pp. 129–131.

(11) Rogers, D. B.; Shannon, R. D.; Sleight, A. W.; Gilson, J. L. Crystal Chemistry of Metal Dioxides with Rutile-Related Structures. *Inorg. Chem.* **1969**, *8*, 841.